Nickel doped zinc oxide electron transport layer for improved performance of P3HT: PC71BM based Inverted Organic Solar Cell

Tewodros Zewdu Wele

A Thesis Submitted to The Department of Materials Science and Engineering

School of Mechanical, Chemical, and Materials Engineering.

Presented in Partial Fulfillment of the Requirement for the Degree of Master's in Materials Science and Engineering

Office of Graduate Studies

Adama Science and Technology University

June, 2023

Adama, Ethiopia

Nickel doped zinc oxide electron transport layer for improved performance of P3HT: PC71BM based Inverted Organic Solar Cell

Mr. Tewodros Zewdu Wele

Advisor: Dr. Dinsefa Mensur Andoshe

Co- Advisor: Dr. Newayemedhin Tegegne Aberra

A Thesis Submitted to The Department of Materials Science and Engineering

School of Mechanical, Chemical, and Materials Engineering

Presented in Partial Fulfillment of the Requirement for the Degree of Master's in material science and engineering

Office of Graduate Studies

Adama Science and Technology University

June, 2023

Adama, Ethiopia

Declaration

I hereby declare that this Master Thesis entitled "**Nickel doped zinc oxide electron transport layer for improved performance of P3HT: PC71BM based Inverted Organic Solar Cell**" is my original work. That is, it has not been submitted for the award of any academic degree, diploma, or certificate in any other university. All sources of materials that are used for this thesis have been duly acknowledged through citation.

Name of the Student	Signature	Date

Recommendation

I/we, the advisor (s) of this thesis, hereby certify that I/we have read the revised version of the thesis entitled "**Nickel doped zinc oxide electron transport layer for improved performance of P3HT: PC71BM based Inverted Organic Solar Cell**" prepared under my/our guidance by Tewodros Zewdu Wele submitted in partial fulfillment of the requirements for the degree of 9Masters of Science in Materials Science and Engineering**.** Therefore, I/we recommend the submission of revised version of the thesis to the Department following the applicable procedures.

Main Advisor	Signature	Date
Co-Advisor	Signature	Date

Approval sheet

I/we, the advisors of the thesis entitled "**Nickel doped zinc oxide electron transport layer for improved performance of P3HT: PC71BM based Inverted Organic Solar Cell**" and developed by Tewodros Zewdu Wele hereby certify that the recommendation and suggestions made by the board of examiners are appropriately incorporated into the final version of the thesis.

Main Advisor	Signature	Date

We, the undersigned, members of the Board of Examiners of the thesis by Tewodros Zewdu Wele have read and evaluated the thesis entitled "**Nickel doped zinc oxide electron transport layer for improved performance of P3HT: PC71BM based Inverted Organic Solar Cell**" and examined the candidate during the open defense. This is, therefore, to certify that the thesis is accepted for partial fulfillment of the requirement of the degree of Master of Science in Material science and engineering.

Chairperson	Signature	Date
Internal Examiner	Signature	Date
External Examiner	Signature	Date

Finally, approval and acceptance of the thesis are contingent upon the submission of its final copy to the Office of Postgraduate Studies (OPGS) through the Department Graduate Council (DGC) and School Graduate Committee (SGC).

Department Head	Signature	Date
School Dean	Signature	Date
Office of Postgraduate Studies, Dean	Signature	Date

Acknowledgement

First and foremost, I am grateful to my research advisors, Dr. Dinsefa Mensur Andoshe and Dr. Newaymedhin Abera Tegegn, for assisting me throughout the research process. Throughout our work, your visionary views, skilled counsel, and consistent inspiration have been essential. The project was a success due to your ability to bring a fresh perspective on the subject matter and assist me in navigating the difficult research methods.

I would also want to thank my colleagues Eyob Shewamen, Kidan G/Egziabher, Biruk Alebachew, Mintesinot Tamiru, Bisrat Nigussie, Lemma Tirfe, and Alemayehu Girma for their help during this project. This project would not have been possible without your involvement and combined efforts. Your willingness to share resources, communicate ideas, and offer helpful input at all stages of the study was critical to giving a thorough analysis. Furthermore, your professionalism, ambition, and love for the project industry have served as an inspiration to me.

I'd like to thank ASTU for this opportunity, as well as Dr. Gebisa Bekele and the Technical Staff of the Material Science and Engineering programme, Mr. Demeke Tesfaye. I'd like to convey my heartfelt appreciation to Dr. Fikadu Gashaw, Head of Physics at Addis Ababa University, for his continuous support and advice during my study. The Institute also has been quite helpful in providing me with tools and facilities that are critical to the success of my study. Last but not least, I'd want to express my gratitude to my long-time classmates, family, and those who have assisted me in some manner.

Table of Contents

List of Tables

List of Figures

List of Abbreviations

AM1	Air mass factor
BHJ	Bulk-heterojunction
BHJSCs	Bulk heterojunction solar cells
CB	Conduction Band
ETL	Electron transport layer
FF	Fill factor
HOMO	Highest occupied molecular orbital
HTMs	Hole transport materials
IOSCs	Inverted Organic solar cells
ITO	Indium Tin oxide
LUMO	Lowest unoccupied molecular orbital
MoO_3	Molybdenum trioxide
Ni-ZnO	Nickel doped Zinc Oxide
OSCs	Organic solar cells
P3HT	Poly (3-hexylthiophenes)
PC71BM	Phenyl C71-butyric acid methyl ester
PCE	Power conversion efficiency
PL	Photoluminescence
QE	Quenching Efficiency
R_s	Series resistance
R_{sh}	Shunt resistance
VB	Valence band
WF	Work function
XRD	X-ray diffraction
ZnO	Zinc Oxide

Abstract

Zinc oxide (ZnO) is one of the widely used electron transport layers (ETLs) for organic solar cells (OSCs). In this study, Nickel doped zinc oxide (ZnO:Ni) thin films were prepared by using a simple sol gel technique by varying the Nickel concentration (2%,3% and 5% by mole) and used in inverted organic solar cells. The thin films exhibited better optical, structural and morphological properties upon nickel doping. Furthermore, a device with a 3 mol.% Ni dopant had the highest power conversion efficiency (PCE) of about 3.72 %, which is 50% higher than the PCE of the ZnO-only device (2.48%). The improved electrical conductivity, short circuit current, fill factor, charge generation and exciton dissociation are the primary reasons for the PCE enhancement. Furthermore, the ETL's increased electrical conductivity by more than one-fold increases the photocurrent from 9.6 to 13.6 mA/cm^2. In addition, due to improved morphology of Ni:ZnO thin films, the fill factor increased by more than 14%. As a result, Ni doping could be a promising, low-cost approach to improve the performance of inverted OSC.

Keywords: *Organic solar cells, Power conversion efficiency, Ni-doped Zinc Oxide, Electron Transport Layer.*

CHAPTER ONE

1.1 Introduction

As the world's energy consumption continues to rise at an alarming rate, the demand for a sustainable and renewable energy source is more urgent than ever. The harmful impact of greenhouse gas emissions caused by the use of fossil fuels has also raised environmental concerns (Zhenghao Hu et al., 2020). The use of abundant and renewable solar energy has been acknowledged as a potential solution to meet the rapidly increasing global energy demands and to combat the environmental issues related to the emission of greenhouse gases from the consumption of fossil fuels. As a result, research in the field of solar energy is currently at the forefront of developing a renewable and carbon-free energy source. Different techniques have been proposed and extensively studied to harness solar energy, such as solar thermal energy, photocatalytic and photo-electrochemical water splitting, and solar cells (Demirbas, 2017; Manju & Sagar, 2017).

Among these technologies, Solar cell technology converting sunlight directly into electricity using semiconductor materials, is considered as one of the most promising and mature technologies. With ongoing advancements in solar cell technology, there is a growing potential to improve their efficiency and reduce their cost, making them a more accessible and affordable energy solution for everyone (Lloyd-Jones et al., 2019). Although silicon-based or other inorganic semiconductor solar cells and thin-film solar cells have been the most commonly used solar cell systems due to their exceptional performance in terms of high efficiency and reliability. However, their high cost and slow energy payback time of these solar cells have limited their widespread applications. The high cost of inorganic semiconductor solar cells and thin-film solar cells is primarily due to the complex manufacturing process and the need for specialized materials. The cost of producing these solar cells can be a significant barrier for many individuals or businesses, particularly in developing countries where the demand for energy is high. Furthermore, the slow energy payback time of these solar cells is another limiting factor. It takes a considerable amount of time for these solar cells to generate enough energy to offset the energy consumed in their production. This can have a significant impact on the overall sustainability of these solar cell systems (Hau, Yip, & Jen, 2010; Gang Li et al.,

2005; G. Li, Zhu, & Yang, 2012; Po, Carbonera, Bernardi, & Camaioni, 2011). As a result, researchers are exploring alternative solar cell technologies that can offer improved cost-effectiveness and energy efficiency. Over the past few decades, there has been a significant amount of research dedicated to organic solar Cells (OSCs) due to their remarkable features such as their lightweight nature, flexibility, and their ability to be manufactured through low-cost roll-to-roll processing techniques (W. Song et al., 2021). The standard type of OSCs, known as bulk-heterojunction (BHJ) OSCs, typically consists of a photoactive layer that is made up of a blend of electron-donating conjugated polymers and electron-accepting fullerene (or non-fullerene) derivatives. This particular composition of materials is highly effective in absorbing sunlight and generating excitons, which can then be separated at the interfacial layer, ultimately leading to the production of photocurrent (Z. Hu, Ying, Huang, & Cao, 2017). OSCs have advanced so far in the past decade that power conversion efficiencies of more than 18% are now regularly reported (Zou et al., 2022).

Bulk heterojunction cells can be made in both conventional and inverted configurations. Despite their high PCEs, conventional OSCs have some drawbacks, including a lack of long-term stability when exposed to air and an acidic PEDOT:PSS interfacial layer that directly contacts and may erode the ITO glass (Wu, Yu, Shi, & Li, 2019). This limits the practical deployment of conventional solar cell devices. Inverted organic solar cells (IOSCs) have been created to address these issues (Lee et al., 2016). The top electrode in traditional OSCs is replaced with an air stable high-work-function metal (e.g., Au or Ag) in this case. Meanwhile, PEDOT: PSS is removed from the device structure, avoiding contact between ITO and PEDOT: PSS. The electron transport layer (ETL) on the other hand, is one of the major reasons limiting OSC performance. ETLs have been produced using N-type metal oxides such as titanium oxide (TiOx), zinc oxide (ZnO), and tin dioxide (SnO_2) layer in devices.

P3HT: PC71BM: based OSC has received the greatest attention, both in conventional and inverted structures using ZnO as ETL. ZnO's conduction band (-4.4 eV) allows for simple electron transfer from PC71BM (LUMO = -3.7 eV), however, its valence band (-7.8 eV) is substantially lower than P3HT's HOMO (-5.3 eV), preventing hole transmission to the ITO in the inverted configuration. The high energy differential between the conduction band of ZnO and the LUMO of PC71BM (~ 0.4 eV) causes considerable energy loss in the device.

Zinc oxide (ZnO) has been employed widely as an ETL in IOSCs devices because of its high visible light transparency, air stability, strong electron affinity, solution processability, and tunable optical and electrical properties (Park, Lim, Kim, & Jang, 2013; Poduval et al., 2020; Wu et al., 2019). Moreover, its conduction band edge is at around 4.4 eV, which is lower than that of the poly (3-hexylthiophenes) (P3HT) and [6,6]-phenyl- (PC71BM) blend. Moreover, the electron mobility of ZnO is relatively high at around 200–300 $cm^2V^{-1}s^{-1}$ (Homnan et al., 2021). However, there are many inevitable defects in the surface of ZnO nanoparticles prepared by sol-gel method, which will result in the recombination of electron-hole pairs (Moon et al., 2016). To address this issue, several techniques such as high temperature annealing, metallic nanocomposites/nanoparticles, and metal doping have been used and this will go a long way toward improving the performance in OSCs (Poduval et al., 2020; X. Song et al., 2021).

Due to its effectiveness in modifying the optical and electrical characteristics of ZnO semiconductors, elemental doping has been acknowledged as a viable strategy. Doping tactics provide a number of benefits: (1) tailoring the electrical structure, (2) increasing conductivities, (3) reducing defect density, (4) modifying energy levels, and (5) modulating carrier density (X. Song et al., 2021). Particularly, a number of doping elements with varied valence states, such as lithium (Li), aluminum (Al), indium (In), titanium (Ti), and tin (Sn), have improved the electronic characteristics of ZnO (Ambade, Ambade, Mane, & Lee, 2015; Lechêne, Leroy, Tosoni, de Bettignies, & Perrier, 2014; Shin, Lee, Lee, Choi, & Kim, 2010; Junfeng Wei et al., 2018; X. Zhu et al., 2019). Although these element doping techniques can increase carrier mobility in ZnO thin films and increase thickness tolerance, the optical transparency of the ETL is sacrificed because of ionized impurities and high parasitic absorption (especially in the NIR range), which results in a significant loss of light-harvesting for the active layer and further decreased current densities (Jung et al., 2018). In order to produce functional solar cell devices, it is critical to establish a simple and practical elemental doping process that achieves high optical transparency while also improving light harvesting for the active layer.

Based on inorganic chemistry, Nickel (Ni) is a transition metal element which belongs to the 4^{th} period and 10^{th} group in the periodic Table along with Iron (Fe) and Cobalt (Co). It has been recognized as one of the most efficient transition metal dopants due to its remarkable chemical stability and ability to change the electrical, optical, and magnetic performance of ZnO

nanostructures (Yilmaz, 2014). Because the bond energy of Ni-O is greater than that of Zn-O, Ni doping might regulate the production of oxygen vacancies (Prerna et al., 2020). The electronegativity of nickel is in comparison average, indicating an adequate affinity for forming bonds with other elements. Nickel is also good conductor of heat and electricity. Moreover, because Ni^{2+} (0.69 Å) has a similar ionic radius to Zn^{2+} (0.74 Å) and has the same valence, Ni^{2+} is expected to replace Zn^{2+} in the ZnO lattice without affecting the hexagonal wurtzite crystal structure (Ali, Khan, Karim, Rahman, & Kamruzzaman, 2020). It is expected that Ni doped ZnO thin films may be a promising material for obtaining a very good electrical, opto-electronic and visible luminescence properties.

In this study, an inverted organic solar cell based on P3HT: PC71BM as the active layer and room temperature sol-gel processed Ni-doped ZnO as the ETLs with different Ni concentrations (0, 2, 3, and 5 mol%) was developed. To the best of our knowledge, no study has been published that uses Ni-doped ZnO as an ETL for P3HT: PC71BM organic solar cells. The addition of Ni to ZnO ETL increased the PCE of P3HT: PC71BM-based OSCs by 50 % compared to an undoped device (2.48%). Electrical and optical spectroscopic techniques were utilized to study the reason for this improvement. Furthermore, charge generation and electron mobility were investigated in order to determine the mechanism for PCE improvement. The results show that improved PCE from Ni doping of ZnO was driven by a synergistic impact of improved conductivity (which increases photocurrent), absorbance, and fill factor.

1.2. Statement of the problem

ZnO thin films prepared using the sol-gel technique at low temperatures have a significant potential for good-quality ETL in OSC devices due to their excellent properties, such as the absence of pinholes, ease of production, thickness controllability, low temperature processing capability and high optical transparency. ZnO films prepared at low temperatures, however, have reduced charge mobility and electrical conductivity due to the presence of numerous surface defect states and intergap energy levels, leading to a decline in photovoltaic performance. To address this issue, Ni was added as a dopant into ZnO ETL due to its high electrical conductivity and similar ionic radius, such that Ni^{2+} replaces some of the Zn^{2+} ions without affecting the crystal structure of the host. Furthermore, there is still no documentation of Ni-doped ZnO as the ETL in P3HT-PC71BM based OSCs. This research sets the path for

further advancements in the performance of organic solar cell by including Ni-doped ZnO as an ETL.

1.3. Objectives

1.3.1 General objective

The fundamental objective of this study is to improve the photovoltaic performance of the P3HT-$PC_{71}BM$ based OSC through the development of Ni-doped ZnO ETL films with varied Ni concentrations in the ZnO structure.

1.3.2 Specific Objectives

This study aims to achieve the following specific objectives:

- Synthesize undoped and Ni-doped ZnO solutions by sol-gel technique with different Ni concentrations, i.e., 2%, 3%, and 5% by mole, and spin coat of the as prepared solution on glass substrate to prepare film.
- Characterize the as-prepared films structural, morphological and optical properties using XRD, SEM, UV-Vis and PL respectively.
- Fabricate inverted BHJ OSC with a device structure of ITO/Ni-ZnO/P3HT: $PC_{71}BM$/ MoO3/Al characterizing and analyzing the Current density versus Voltage (J–V) characteristics of the fabricated i-OSC devices.
- Determine the electron mobility and charge generation of the as fabricated devices.

1.4. Significance of the study

The need for efficient and sustainable energy sources is urgent considering the rising global energy consumption. Global energy consumption has increased by more than four times in the past forty years, and as of 2019, it is estimated to be over 18.5 terawatt years each year (Sutton, 2018). With the rapid rise in global energy consumption, it is estimated that coal, oil, and natural gas-based world energy would expand by an average of 0.6% per year between 2015 and 2040. However, these energy sources emit CO_2, which is a major contributor to human greenhouse gas emissions globally, resulting in rising global temperatures. A large portion of Ethiopia's population lives in rural areas, with only a few having accesses to electricity. Hydropower generates over 96% of Ethiopia’s electricity, while biofuels meet the majority of the country's energy needs for cooking, heating, and off-grid lighting. Ethiopia, on the other hand, plans to

replace these energy sources with carbon-neutral alternatives by 2025 (Eshete, Mulatu, & Gatiso, 2020). Given the aforementioned issues, this research is critical in establishing the foundation for delivering clean energy to our community through the use of environmentally friendly, safe, and long-term solar energy.

1.5. Scope of the study

The study is limited to modifying ZnO ETL with Ni doping in inverted OSC to satisfy the research objectives.

CHAPTER TWO

2. Literature Review

2.1. Solar Energy

One of the most pressing challenges of the twenty-first century is preventing an energy crisis. As a result, energy consumption is rapidly rising to fulfil the needs of the world's growing population. Different countries in the world have their own strategies, plans, policies, and control measures in place to establish themselves in the world. The world's resources are depleting as a result of population increase and development activities (Shafiee & Topal, 2009). It is therefore critical to pursue environmentally friendly energy sources in order to improve the world's future. Consideration should be given to renewable energy sources such as solar energy, wind energy, hydropower, and geothermal since they are ecologically benign. (Herzog, Lipman, & Kammen, 2001). However, solar energy may be the best option for the future world for a number of reasons: First, solar energy is the most abundant renewable energy source; the sun emits it at a rate of 3.8×10^{23} kW, with the earth intercepting around 1.8×10^{14} kW. Solar energy reaches Earth in several forms, including heat and light. The majority of this energy is lost as it travels owing to cloud dispersion, reflection, and absorption. According to studies, solar energy can fully supply the world's energy needs because it is abundant in nature and a free source of energy (Lewis, 2007). Second, it is a promising source of energy in the globe since it is not exhaustible, providing solid and rising production efficiency over other energy sources.

The distribution and intensity of solar radiation are two critical factors influencing the efficiency of the solar PV industry. Such two variables vary greatly across countries.

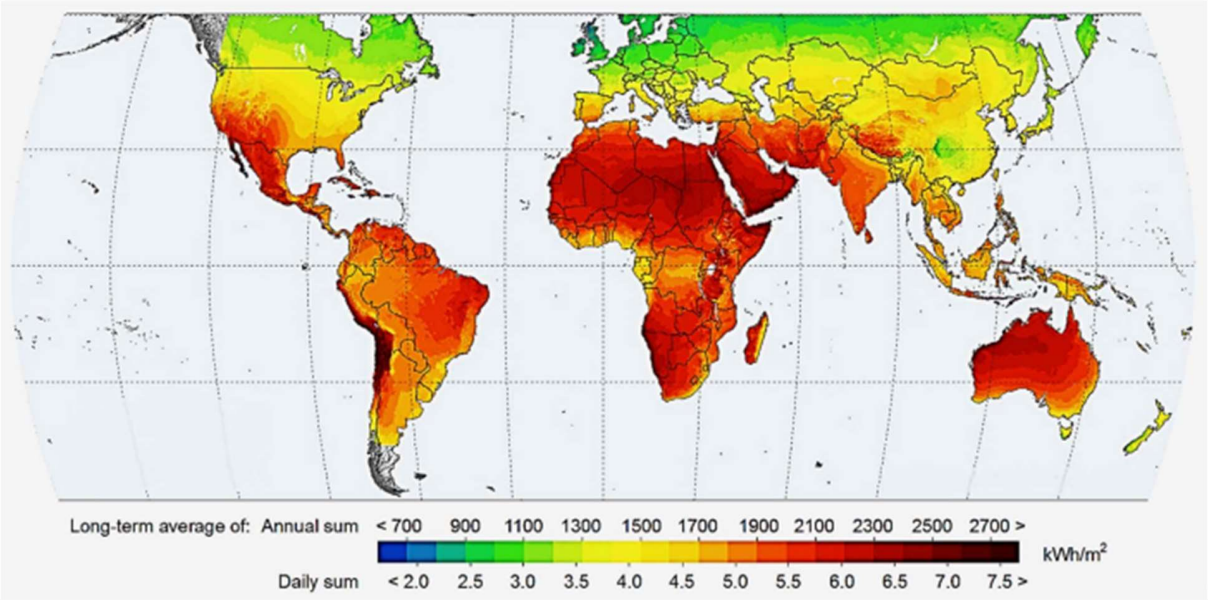

Figure 1 Maps of global horizontal irradiation (GHI) (Martinez-Lozano et al., 1984).

Third, the use and tracking of solar energy have no negative effects on ecosystems in which natural balance is maintained for the benefit of living organisms. Exploitation of fossil fuels harms ecosystems, which in turn harms natural balance. Fourth, because solar systems are relatively inexpensive and practical, they may be used efficiently for village systems, industrial activities, and households. Furthermore, the world is now in a race to find solar energy due to the increasing reliance of the global population on fossil fuels for energy recovery in order to perform various activities. The right application of this technology would be the best alternative for the future world to prevent the negative consequences of an energy crisis. Many studies are currently being conducted in order to improve the efficiency of the solar industry in order to make the future world more productive in terms of energy utilization (Schlamadinger et al., 1997).

The distribution of solar radiation is represented by the solar spectrum, which is made up of continuous radiation. Figure 2 illustrates that the measured spectrum does not quite match the blackbody curve. The solar spectrum of the upper atmosphere is essentially equivalent to a black body (black line) at 5250°C. Solar radiation is broadly related to blackbody radiation in the visible and infrared bands at 5250°C; however, in terms of equivalent blackbody temperature in the Sun, ultraviolet (UV) solar radiation differs substantially from visible and

infrared radiation (Lewis & Nocera, 2006). The number of deviations or discontinuities of solar radiation observed on earth at sea level, Figure 2 (red spectrum). These deviations or discontinuities are mainly due to the absorption of radiation by various molecules in the atmosphere, such as water vapor (H_2O), carbon dioxide (CO_2), nitrous oxide (NO_2), methane (CH_4), fluorocarbons and dust, oxygen (O_2) and ozone (O_3), etc (Markham & Barker, 1987). Furthermore, air scattering is critical in removing high frequencies from direct sunlight and scattering across the sky. The air mass factor AM, which is defined as the path length that sunlight takes through the Earth's atmosphere, can be used to estimate the effect of the atmosphere on the solar spectrum and power incident density. AM0 denotes the spectrum outside the atmosphere, and AM1 denotes the spectrum of normal incidence on the earth's surface. The typical spectrum of an ordinary climate is AM1.5, which corresponds to a solar radiation angle of incidence of 48° as compared to a normal surface. In the mid-latitude area in summer, the AM number is less than 1.5 times, and the number is significant in the morning and evening and at other times of the year. As a result, AM 1.5 can be used to describe the total annual average of mid-latitude locations (Würfel, Wagner, & Hinsch, 2005).

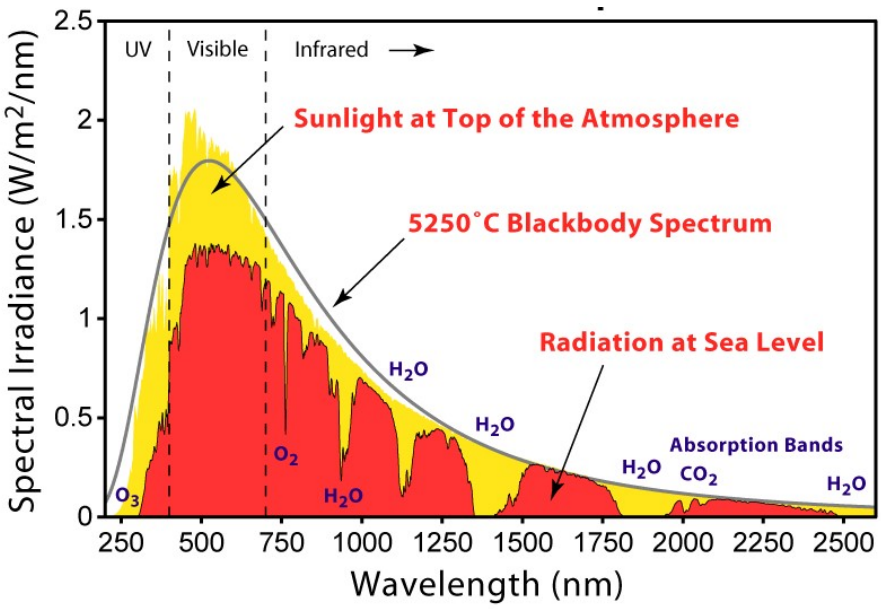

Figure 2 The solar spectrum (Houshyani Hassanzahed et al., 2007).

2.1.1 Photovoltaic Technology

Photovoltaic devices commonly use semiconductor material to induce electricity, with silicon being the most commonly used. This device works by providing extra energy to activate electrons. This device operates on the principle that electrons are activated from a lower energy state to a higher energy state as a result of energy addition from sunlight. This activation produces a large number of holes and free electrons in the semi-conductor, resulting in electricity (Green, 2002). Multi-junction cells, mono-crystalline silicon solar cells, poly-crystalline silicon solar cells Amorphous thin film, cadmium telluride (CdTe), copper indium gallium selenium (CIGS), copper zinc tin sulphide, organic and dye sensitized solar cells are good examples of photovoltaic systems.

2.2 Organic solar cells (OSCs)

Organic solar cells (OSCs) have gotten a lot of attention since they are easy to make, lightweight, semi-transparent, flexible, and cheap. In the previous two years, advances in the creation of innovative organic materials, surface shape, and suppressed saturation current have increased the power conversion efficiency (PCE) of OSCs from 12% to over 17% (see figure 3) (Meng et al., 2018). An organic solar cell typically has three layers: an active layer in the middle, an electron transport layer (ETL), and a hole transport layer (HTL) on each side to aid in charge movement and electrodes at the bottom and top to collect the charges. The ETL and HTL are essential to transmit electrons and holes generated by the active layer to each electrode effectively (Van Le, Choi, & Kim, 2017). ZnO is the most often employed electron transport layer (ETL) in OSCs with an inverted device configuration. ZnO is an II-VI material that has a wide range of uses, including solar cells, light-emitting diodes, sensors, piezoelectric devices, and photocatalysts (Z. L. Wang, 2009).

Because of its strong electron conductivity and low hole conductivity, it is an attractive ETL for thin-film solar cells. It should be noted, however, that ZnO has been demonstrated to have a significant photosensitivity because to the existence of surface imperfections (Polydorou et al., 2022). Doping can readily tune the bandgap and electrical conductivity of low work function ZnO (Özgür et al., 2005). The electrical characteristics of an n-type semiconductor can be converted to a metal-like degenerate semiconductor by manipulating the dopants without considerable loss of optical transparency. The Moss-Burstein effect, caused by larger carrier

concentrations in degenerately doped ZnO, can also increase the optical bandgap and short-wavelength transparency (Suwanboon, Amornpitoksuk, & Sukolrat, 2011).These characteristics make doped ZnO films for solar cell applications very interesting.

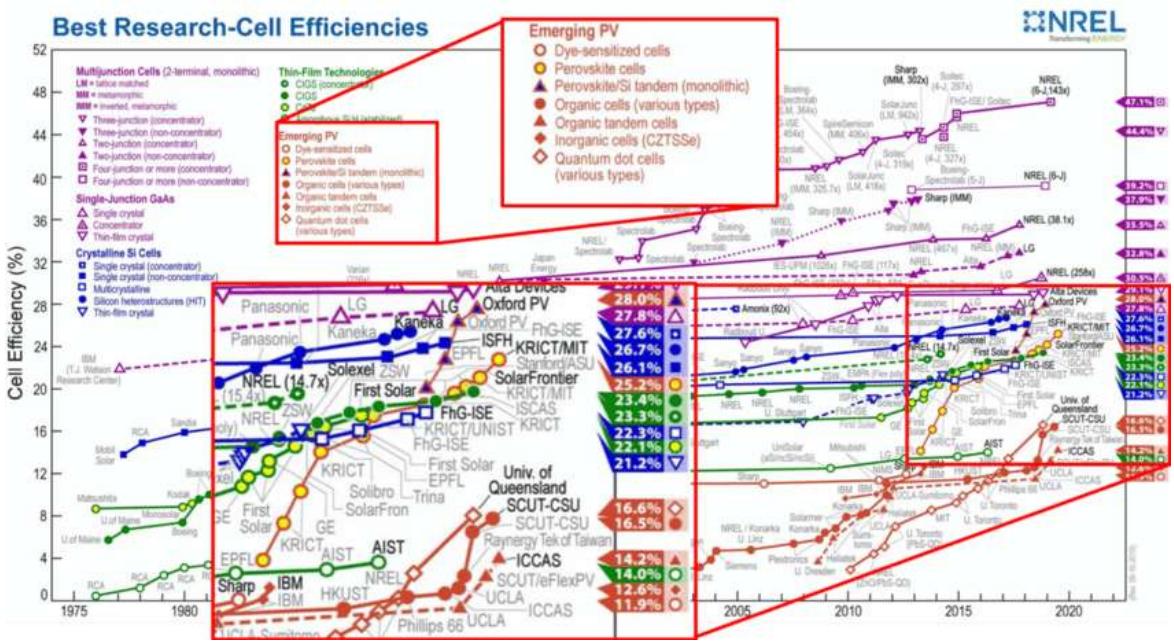

Figure 3. The new version of the Best Research-Cell Efficiency Chart (Image: Screenshot, NREL)

2.2.1 Working principles of organic solar cells.

Figure 4 displays the well-known operating mechanism of BHJ OSCs. The donor and acceptor materials must first absorb the incident photons in order to produce excitons, which are essentially electron and hole pairs. These excitons subsequently diffuse towards the donor-acceptor contact, where they split into electron and hole moieties after defeating the Coulomb interaction force. Finally, these independent electrons and holes move in the direction of the cathode and anode, respectively, and are gathered by the corresponding electrodes. It is generally accepted that one of the most significant factors influencing device performance is the choice of the proper active layer materials. Such materials have evolved through three stages over the last few decades. The famous poly(3-hexylthiophene) (P3HT) donor and fullerene acceptor were essentially combined in the first-generation materials, and the resulting devices were capable of achieving PCEs of about 5% (G Li et al., 2005). A significant improvement in the performance was later noticed as PCEs of over 11% were obtained following the

development of D-A copolymer systems and creating corresponding blends with fullerene derivatives (Zhao et al., 2015).

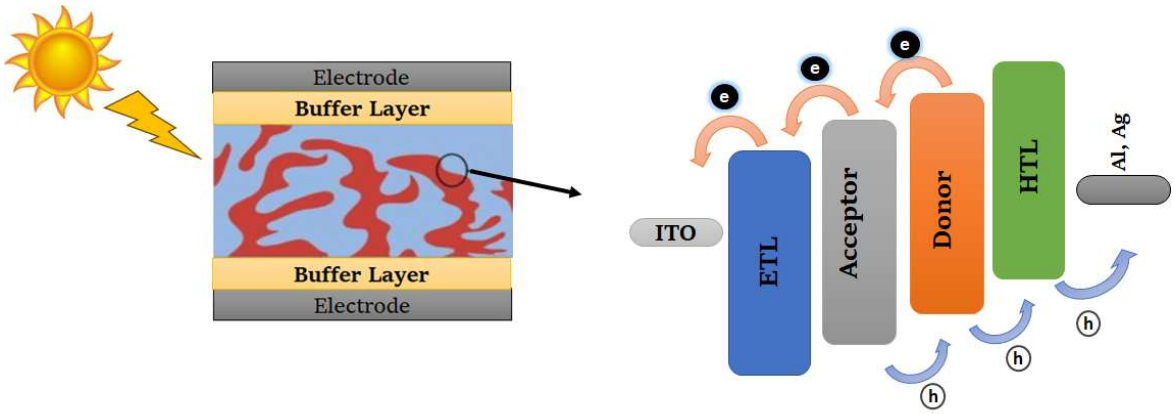

Figure 4. The operating mechanism of OSCs (G. Wang, Melkonyan, Facchetti, & Marks, 2019).

2.2.2. Device configuration in bulk heterojunction solar cells (BHJSCs).

In OSCs, there are two device configurations: conventional and inverted geometries, as seen in Figure 5. As stated in the introduction, the conventional structure consists of a transparent electrode (ITO) at the bottom for hole collection, followed by deposition of hole transport layer (HTL) as anode buffer or interfacial layer and then a thin layer of active material, followed by deposition of electron transport layer (ETL) as a cathode buffer or interfacial layer, and finally a top metal electrode as a cathode for electron collection.

Except for the location of ETL and HTL, the same holds true for inverted device architectures. The roles of the electrodes are reversed in the inverted structure (Figure 5b), so electrons are collected by the bottom transparent electrode and holes by the top metal electrode, whereas in the conventional structure, holes are collected by the bottom electrode and electrons by the top electrode. Due to the reversed collection, the work function of the top electrode must be high enough to match the donor's highest occupied molecular orbital (HOMO) energy level, while the bottom electrode must have a work function low enough to match the acceptor's lowest unoccupied molecular orbital (LUMO) (Facchetti, 2013). While high work function metals such as gold or silver can easily meet the top metal electrode requirement, the correct selection of the bottom electrode is more difficult. In fact, the most commonly used transparent metal

oxides, such as ITO or FTO, have high work functions that do not match well with the acceptors' LUMO level (Rafique, Abdullah, Sulaiman, & Iwamoto, 2018). By altering the bottom electrode and depositing a thin layer of appropriate electron-conducting (hole blocking) materials, such as ZnO, which is the most widely used and transparent to visible light, the energy levels are matched. Because of the rapid oxidation of the low WF metal, conventional device construction presents issues with device stability in air and/or moisture. Due to its acidity, PEDOT:PSS, for example, may quickly damage the ITO electrode, reducing device stability over time (Bolognesi, 2013).

Furthermore, the inclusion of an air-sensitive ETL in a typical device structure makes the manufacturing process difficult to perform in air, necessitating the use of thermal evaporation methods under vacuum, increasing the complexity and fabrication cost of these devices. The inclusion of an air-sensitive ETL in a standard device structure makes it difficult to fabricate the device in air, necessitating the use of thermal evaporation procedures under vacuum, increasing the complexity and fabrication cost of these devices (H.-C. Chen, Lin, Jiang, Su, & Wei, 2015). Inverted device designs, which are also used in this thesis, have recently gained a lot of attention due to their higher stability when compared to conventional devices. The higher WF metal electrode (such as Au and Ag) in this configuration is more resistant to air and moisture oxidation, overcoming one major hurdle for possible widespread application of organic solar cells and increasing overall cell durability (Sasajima, Uesaka, Kuwabara, Yamaguchi, & Takahashi, 2011).

Furthermore, inverted device structures have been developed to address the issues associated with the air sensitivity of ETL in a traditional device structure by reversing the transport direction of electrons and holes by using a metal with a high work function as the anode on top of a device with ITO as the cathode at the bottom. Furthermore, in the case of inverted solar cells, the high-work-function metal anode, such as Ag, can be prepared using either coating or printing technology, both of which are compatible with all solution processing and can thus greatly simplify and reduce solar cell manufacturing costs (Krebs, 2009). Another advantage of inverted geometry over conventional geometry is that it provides for greater flexibility in the design of multi-junction or tandem solar cells. Because of the vertical phase separation mechanism that characterizes the P3HT prone to accumulate on the electrode top and the

fullerene derivative on the bottom, the inverted device arrangement is also more beneficial than the conventional configuration (L. M. Chen, Hong, Li, & Yang, 2009).

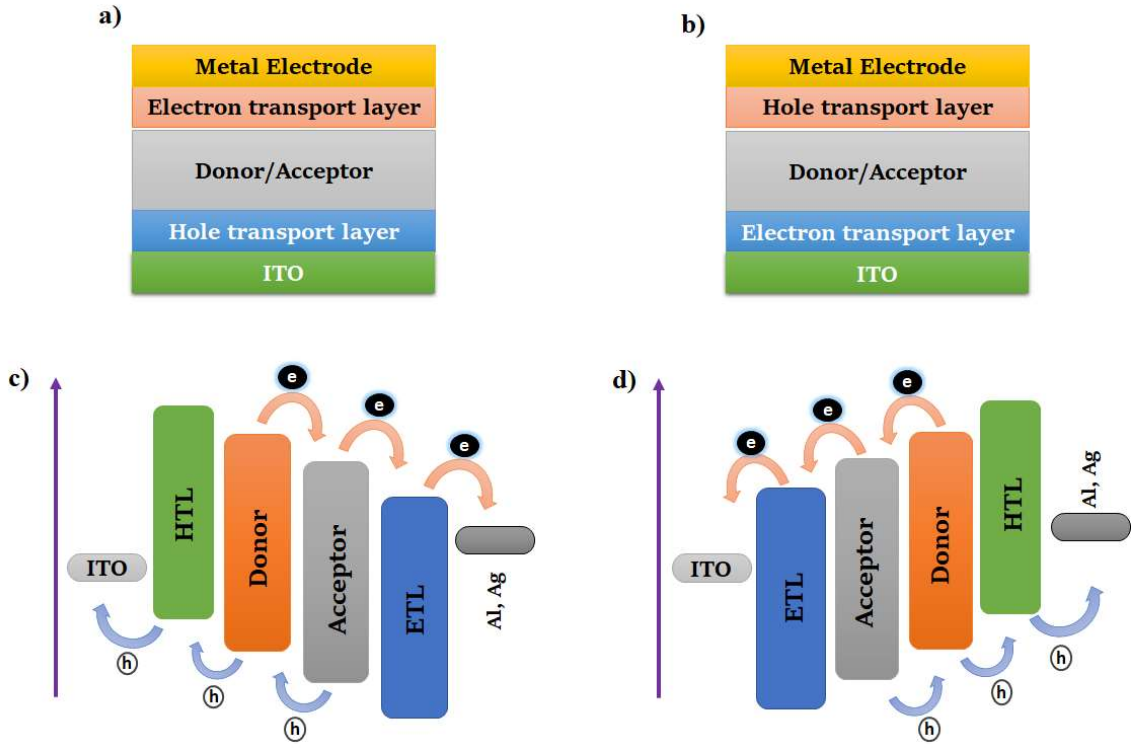

Figure 5. Conventional (a), inverted (b) structures of OSCs; (Z. Hu et al., 2017) Schematic illustration of the energy level diagram and the charge transport direction of the (c) conventional devices and (d) inverted devices (X. Xu & Peng, 2022).

2.2.3. Photovoltaic parameters

The ability of an organic solar cell to convert light to electrical energy is reflected in the current density (Jsc) as a function of the voltage, (V) under illumination conditions, and the photovoltaic parameters that determine the efficiency of the solar cell can be extracted from these curves, as shown in Figure 6 The photovoltaic parameters are summarized here.

A short circuit current (J_{sc}) is the current that flows through a solar cell when the applied voltage is zero, or it reflects the number of charge carriers created and eventually collected at the corresponding electrodes at zero applied potential. J_{sc} is primarily determined by the material's capacity for light absorption and to produce excitons, which is influenced by its absorption coefficient, band gap, and exciton diffusion at the donor/acceptor interface, which varies with

the materials' exciton diffusion lengths. On the other hand, open circuit voltage (V_{oc}) is the highest voltage that a solar cell can extract for an external circuit or the voltage when there is no current flowing through a solar cell under light irradiation. The measure of the squareness of the J-V, or the ratio of maximum power to the product of open-circuit voltage and short-circuit current, is known as the fill factor and is given by the equation:

$$FF = \frac{Vmax \times Imax}{Voc \times Jsc} \qquad (1)$$

Where V_{max} and I_{max} are the voltage and the current at the maximum power (P_{max}) point respectively.

Solar cell power conversion efficiency is defined as the ratio of a solar cell's electrical output to the incident light power to which it is exposed.

$$\eta = \frac{Pout}{Pin} = \frac{FF\ (Voc \times Jsc)}{Pin} \qquad (2)$$

Where P_{out} and P_{in} represent the output and input power respectively.

While the other hand, Maximum power (P_M) is the amount of electric power that an OPV cell can generate when illuminated.

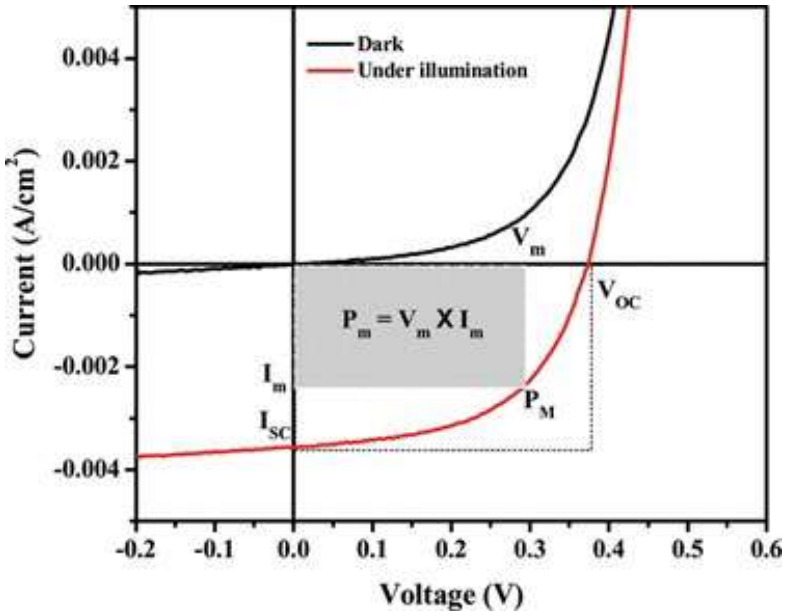

Figure 6. J-V characteristic curve schematic representation of OSC (Abdulrazzaq, Saini, Bourdo, Dervishi, & Biris, 2013).

2.2.4 Mechanisms Behind Degradation/Instability

The stability of OSC devices is the most significant element that should be given special attention in order to commercialize them, despite the fact that there has been little literature on the stability of OSCs in comparison to the literature on the efficiency of OSCs. A study of the stability of OSCs aids in understanding how a device degrades throughout operation (Rafique et al., 2018). Device instability develops as a result of a variety of complex events at work at the same time. Mechanical stress, irradiation (duration and intensity), water, oxygen (Air effect), burn in degradation, thermal effect, and other degrading variables (Fig 7) may impact the active layer, transport layers, contacts, and the interface of each layer with the surrounding layers.

In general, degradation factors in OSCs can be classified as intrinsic, which occurs due to thermal diffusion of constituent materials at OSC interfaces (Ghasemi et al., 2021) or extrinsic, which occurs due to changing environmental conditions (light, dark, hot, cold, dry, and humid conditions), and includes oxygen and water, irradiation, mechanical stress, and so on.

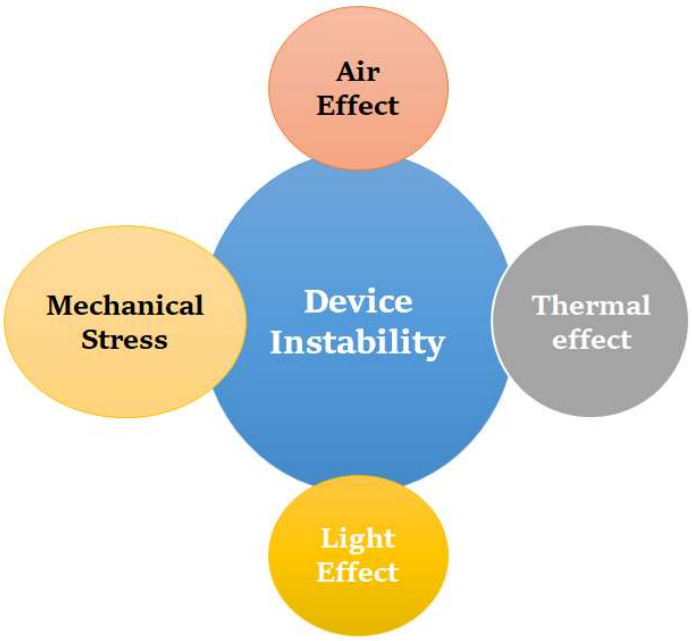

Figure 7. Schematic diagram of mechanisms behind the instability of OSCs. Each of these factors influence the degradation of OSCs (Duan & Uddin, 2020).

2.3. Hole and Electron Transport Layers in Organic Solar Cells

OSCs are generally made up of a BHJ active layer sandwiched between a transparent bottom electrode and a top metal electrode. In theory, the two electrodes' distinct work functions (WF) create a built-in electrical field in the device that drives photogenerated free charges to the respective electrodes, where electrons are extracted by the lower WF electrode (cathode) and holes are extracted by the higher WF electrode (anode) (Chueh, Li, & Jen, 2015). In a typical OSC device, the bottom transparent electrode is indium tin oxide (ITO, WF=4.8 eV), and the metal electrode is aluminum (Al, WF=4.3 eV) or argentum (Ag, WF=4.4 eV). The WFs of these electrodes are insufficient to match the majority of highly efficient donor and acceptor materials, resulting in an insufficient built-in electrical field and severe voltage loss of the devices. Non-Ohmic connections between the active layer and electrodes, on the other hand, create substantial energy barriers at the interfaces, hindering charge extraction from the active layer to the electrodes. Significant effort has been put into interfacial engineering to avoid these issues (H. Xu et al., 2020). By inserting a proper hole transporting layer (HTL) between the BHJ layer and the anode, as well as an electron transporting layer (ETL) between the BHJ layer and the cathode, the WF can be fine-tuned and the interfacial contact optimized, forming favorable cascade energy alignment and contributing to significantly improved charge extraction efficiency and photovoltaic performance (Figure 5 (c) and (d)). HTL and ETL involved device topologies are now the canonical paradigm for extremely efficient OSCs.

2.3.1. Hole transport layer materials

The hole is collected or extracted from the absorber layer by the HTL, but electrons must be blocked.

Hole transport materials (HTMs) play a crucial role in the overall performance of solar cell devices, and researchers must consider the following prospects for the introduction of novel HTMs. It must have adequate energy levels to provide the driving force for charge transfer, which implies that the highest occupied energy level, i.e., the highest occupied molecular orbital (HOMO) energy levels of the chosen HTMs must be somewhat higher than that of the BHJ materials (Litzov & Brabec, 2013). Furthermore, it should serve as a barrier between the anode

and the active layers, preventing electrons from entering the anode. A good HTM must meet four important criteria: high hole mobility, ideal HOMO energy level, strong solubility and film-forming characteristics, and inexpensive cost. There are three types of HTL: organic, inorganic, and carbonaceous. The organic-based HTL consists of a long-chain polymer and tiny molecules that are almost polymeric in nature. Nickel-based, copper-based, p-type semiconductors, and transition metal HTMs are examples of inorganic HTL (Pitchaiya et al., 2020). However, the most commonly used HTLs in BHJ SCs are polymers, like PEDOT: PSS, or metal oxides, like MoO_3, V_2O_5, WO_3, NiO.

Because of its high work function (which closely matches the HOMO level of commonly used donor polymers), high transparency in the visible range (greater than 80%), good electrical conductivity, and ability to reduce ITO surface roughness while increasing work function, PEDOT: PSS is the most widely used HTL in standard geometry BHJ solar cells (Carter, Angelopoulos, Karg, Brock, & Scott, 1997). However, because PEDOT: PSS is very hydrophilic when deposited as the HTL onto hydrophobic organic layers in inverted devices, poor film morphology, and electrical characteristics have been found. High work-function metal oxides and molybdenum trioxide (MoO_3) have already been shown to be appropriate substitutes for PEDOT: PSS. Nowadays,

MoO3, with its huge bandgap of 2.9 to 3.1 eV and high work function of 5.5 eV, is commonly used as the best HTL in OSCs (Ren, Sun, Cui, & Li, 2018).

Developing HTLs based on inorganic materials to replace the traditionally used PEDOT: PSS has also gotten a lot of interest in recent years. Because of their nonacidic and chemically stable characteristics, metal oxides may be viable HTLs. Among metal oxides, MoOx has been widely employed as the HTL, which is frequently deposited using vacuum evaporation. MoOx solution-processing technologies have been developed in recent years to ease the manufacturing process (Jung, Lee, Kim, & Park, 2020). Because of their poor conductivity, MoOx HTLs can only be used in thin layers (10 nm).

In early 2008, Chen and colleagues demonstrated that MoO_3 enhanced the overall efficiency of a BHJ ISC with both a P3HT: PC71BM active layer and a nanocrystalline TiO_2 ETL. To attain the same performance as devices utilizing Ag or Au, the evaporated MoO_3 layer must be thicker when Al is used as the top electrode. According to the literature, this is owing to the chemical

interaction between Al and MoO_3 during the evaporation process, which resulted in the development of a MoO_2 species due to MoO_3 reduction (Tao et al., 2008). The MoO_3 thickness dependence of efficiency has been explained by the works reported by Zheng et al (Yin, Zheng, Chen, & Cai, 2013) and by Wantz and coworkers (Chambon et al., 2012) ,they observed that when the thickness of the MoO3 layer was in the 10-20 nm range, basic device parameters remained essentially same, but when the thickness was lowered to 5 nm, both Voc and FF decreased. Furthermore, they discovered that decreasing the thickness of the MoO_3 layer resulted in both an increase in series resistance and a decrease in shunt resistance when the thickness of the MoO3 layer was lowered. To summarize, the HTL can increase the WF of the ITO anode while decreasing the interfacial energy barrier between the anode and the active layer, allowing for the formation of ohmic contact between the ITO anode and the active layer, block electrons and minimize interfacial charge recombination, physically change the surface of the ITO anode, passivate surface imperfections and pinholes, and reduce leakage current. Finally, the HTL can alter the shape and absorbance of the active layer, as well as the PCE of OSCs (Tu et al., 2016).

2.3.2 Electron Transport Materials

The role of the ETL is to collect electrons from the absorber layer and deliver them to the anode while blocking holes. The following conditions must be met for materials to serve as ETL: the uppermost occupied energy level, HOMO, and the lower unoccupied energy level, LUMO, should be higher and lower, respectively, than that of the active layer, and high transmittance of light over a wider wavelength range to allow a high fraction of light with sufficient energy to reach the active materials in the case of inverted BHJ solar cell devices (Mahmood, Sarwar, & Mehran, 2017). Historically, low WF metals (e.g., Ca, Ba) were frequently utilized as ETLs in a standard device configuration of ITO/poly(3,4-ethylenedioxythiophene): poly (styrene sulfonate) (PEDOT: PSS)/active layer/ETL/Al (or Ag). Low WF metals, on the other hand, are extremely susceptible to oxygen and moisture, giving the devices very little stability in an air atmosphere. To overcome these issues, n-type metal oxides were used as ETLs, and inverted devices of ITO/ETL/active layer/HTL/Al (or Ag) were created. Zinc oxide (ZnO) has been frequently employed as an ETL in fullerene-based OSCs due to its high transparency and conductivity (Y. Han et al., 2021). ZnO ETLs can be made by the nanoparticle technique or the

sol-gel route. Hou et al. has discovered a new technology of printable ZnO as the ETL for flexible OSCs (X. Xu & Peng, 2022).

ZnO ETLs prepared using nanoparticle or sol-gel methods frequently have a high density of recombination centers, resulting in insufficient charge extraction and transport. A few solutions for eliminating the defect effect of solution-processed ZnO films have been developed. Self-assembled monolayers (SAMs), ionic liquids, and functionalized fullerenes, polymer electrolyte (PFN, PFN-Br, and so on) are popular passivators that are coated on the top of the ZnO surface (Zheng et al., 2019). Unfortunately, this layer is relatively thin (often a few nanometers or less), making manufacture of large-area, dense, and compact layers difficult. Furthermore, the defect states in bulk ZnO ETLs are difficult to passivate using this method (C. Z. Li et al., 2016). More importantly, for non-fullerene acceptors, particularly cutting-edge Y6 and its derivatives (absorption range: 600-950 nm), they efficiently harvest the near-infrared (NIR) part to improve device performance across the solar spectrum, which necessitates a wide bandgap with minimal free-carrier absorption in the ETL to avoid parasitic absorption in the red parts of the solar spectrum. Because of the serious intrinsic intragap level and further serious parasitic absorption of ZnO semiconductor, most of the solutions mentioned above cannot overcome this problem (X. Song et al., 2021).

Motivated by these criteria, elemental doping has been recommended as a viable method for changing the optical and electrical properties of ZnO semiconductors. Doping strategies have various advantages:1) adjusting the electrical structure; 2) boosting conductivities; 3) decreasing defect density; 4) changing energy levels; and 5) controlling carrier density (L. Li & Schirra, 2012). Specifically, several doping elements with different valence states, such as lithium (Li), aluminum (Al), indium (In), titanium (Ti), and tin (Sn), have improved the electrical characteristics of ZnO. Although these element doping methods can improve thickness tolerance by increasing carrier mobility in ZnO thin films, the optical transparency of ETL is sacrificed due to ionized impurities and high parasitic absorption (especially in the NIR range), resulting in significant light-harvesting loss of the active layer and further lower current density (Jung et al., 2018).

As a result, in order to construct effective solar cell devices, a simple and convenient elemental doping technique that simultaneously achieves high optical transparency and thickness independence in ZnO ETL is required.

2.3.3. ZnO electron transport layers (ETLs) in inverted Organic solar cells (OSCs)

Numerous researchers have reported ZnO as the ETL in the P3HT: PC71BM and other types of organic and inorganic based devices as a prototype PV system, and PCE is improving over time. The majority of the published work on the use of ZnO as an ETL in inverted OSCs focuses on the design, fabrication, and characterization of ZnO, doped-ZnO, and ZnO-based composite ETLs, as well as their surface chemistry and morphology modification for photovoltaic performance enhancement in inverted Organic solar cells (OSCs).

Doping is a common strategy used in ZnO structures to increase charge collection efficiency and prevent charge recombination caused by charge entrapment by defects or oxygen ions. Doping improves the conductivity and other properties of ZnO, which improves the photovoltaic performance of inverted solar cells. ZnO ETLs in inverted OSCs are typically only a few tens of nanometers thick to provide excellent conductivity, reduce serial resistance, and improve device performance (Stubhan et al., 2011). However, the thin ETL reduces the devices' mechanical robustness and protection against chemical or physical reactions between the active layer and the electrode. The n type characteristics of ZnO can be improved by substituting group III elements like Al(Maldonado & Stashans, 2010), Ga(Moditswe, Muiva, & Juma, 2016), and In(Hafdallah, Ynineb, Aida, & Attaf, 2011) for Zn. These elements' incorporation primarily results in shallow defect levels, which considerably increase ZnO's conductivity. The most widely used material, especially in Si solar cells for its use as a TCO and an ETL, has been Al-doped ZnO.

Shirakawa et al. were the first to demonstrate the use of ZnO film as a cathode interfacial layer in an organic photovoltaic cell with an ITO/ZnO/C_{60}/PAT6/Au stacked structure (G. Yu, 1995). Wang et al. showed that 4.18% efficiency is achieved using 36 nm ALD ZnO plated at 80 °C and capped with Ag on a P3HT:PC71BM OSC (J.-C. Wang et al., 2010). By using thin ALD ZnO topped with an Al electrode on a nickel phthalocyanine (NiPc) without an anode layer, Stakhira et al. demonstrated a 2.5-fold increase in efficiency (Stakhira et al., 2010). When

Frankenstein et al. applied a similar strategy to PCDTBT: PCBM based OSCs, they noticed an increase in efficiency of 2.75 to 3.5% (Frankenstein, Leng, Losego, & Frey, 2019). On the other hand, Kim et al. showed that just 2 nm ALD ZnO improved OSCs' stability and performance (Kim, Kang, Kim, & Kim, 2011). Alstrup, J., et al.,(Alstrup, Jørgensen, Medford, & Krebs, 2010) doped Al to ZnO to increase the conductivity and quality of ZnO films formed using the slot-die coating process. Since it improves device performances and device stability, lithium fluoride (LiF) has been utilized as an ultra-thin layer beneath the top Al electrode in standard configuration bulk heterojunction solar cells for a long time. Li, J., et al., (J. Li et al., 2019) reported various concentrations of Cd-doped ZnO (2.5, 5, and 10%) as the ETLs in inverted organic solar cells built using PTB7-Th:PC71BM as the active layer, and in this research, they recorded that OSCs containing 5% CZO has a short-circuit current (J_{SC}) of 17.15 mA/cm^2, a fill factor (FF) of 69.38 %, and a power conversion efficiency (PCE) of 9.28 %. Internal metal ion doping in ZnO can significantly minimize surface charge recombination and increase electron extraction that leading to improved solar cells performance according to the literature. Yang, Z., et al.,(Yang et al., 2017) utilized and studied Al-doped ZnO (AZO) ETL in the inverted device based ternary blend of polymethine [3,4-b] thiophene/benzodithiophene (PTB7), [6,6]-phenyl C71-butyric acid methyl ester (PC71BM) and indene-C60-bisadduct (ICBA), demonstrated that the use of ZnO/ AZO nanoparticles improves both short and open circuit current (J_{sc}) and voltage (V) resulting in a recorded power conversion efficiency (PCE) of 8.85 % which is due to the lower work function of AZO than ZnO, resulting in a bigger built-in potential across the organic heterojunction and hence more effective photo-current extraction and larger open-circuit voltages According to Krebs et al., Al-doped ZnO (AZO) with an Al-to-Zn ratio of 1% can greatly improve the conductivity of the AZO layer, thus improve device performance (Oh et al., 2011). Furthermore, the remarkable correlation between AZO ETL form and light trapping in inverted OSCs warrants additional investigation. Wei, J., et al. synthesized Sn-doped ZnO (ZTO) from a sol gel solution and used it as an electron transport material in OSCs, discovering that the produced ZTO films had superior charge transport capabilities and smoother surface morphology after Sn alteration, particularly when treated at a low temperature of 120 ^{0}C. Inverted OSCs with high-temperature (200 ^{0}C) treated ZTO films had the maximum power conversion efficiency (PCE) of 9.32%, which was higher than that of ZnO films processed at the same temperature (Jiajun Wei, Yin, Chen, & Zheng, 2017).

The contribution of low-temperature solution-processed ZnO ETLs to improving the performance of inverted OSCs is restricted due to the existence of high-density defects including dangling bonds and surface groups, as well as the poor spatial distribution of nanoparticles over a large region. In order for inverted OSCs to perform well, homogeneous ZnO NPs sheets with low-density flaws must be created. To address such challenges, polymer-modified ZnO films, commonly known as ZnO/polymer hybrids or nanocomposites, have lately been explored. Chen, H.-C., et al., reported polyethyleneimine doped zinc oxide composites (ZnO:PEI) as efficient electron transport layers (ETL) for enhancing electron extraction in inverted organic solar cells, demonstrating the power conversion efficiency (PCE) of the P3HT:PC61BM (1:1, w/w) device improved to 4.6% when a composite of ZnO:PEI (93:7, w/w) was used Figure 8 (a) depicts the inverted BHJ system 1 or 2 device structure they investigated, in which P3HT or PBDTTBO were utilized as the electron donor and PC61BM or PC71BM as the electron acceptor; BHJ systems1 and 2 represent P3HT:PC61BM and PBDTTBO: PC71BM, respectively.

Surface roughness of the ZnO layer improved, as did structural order of ZnO in the ZnO: The explanation for the performance gain was the PEI layer, which considerably increased electron mobility in the vertical direction. (H.-C. Chen et al., 2015). Furthermore, they investigated the passivation effect of PEI modification on surface defects of ZnO films by studying the photoluminescence (PL) spectra (see Figure 8 (c)) of ZnO:PEI films, which showed no apparent emission near 535 nm due to trap emission or surface recombination, indicating that there were very few oxygen vacancy defects (Ye et al., 2005). Figure 8d depicts AFM surface topography pictures of ZnO:PEI composite layers with varied PEI concentrations. The pristine ZnO surface, as well as those with 1% and 9% PEI added, exhibited continuous rough and root-like structures (Figure 8d, (b, f)). Surface roughness was reduced from 6.7 nm for pristine ZnO to 4.6 nm for a 7% PEI in ZnO mix, potentially improving physical contact and establishing strong molecular dipoles between the ITO electrode and the active layer, resulting in better PCEs.

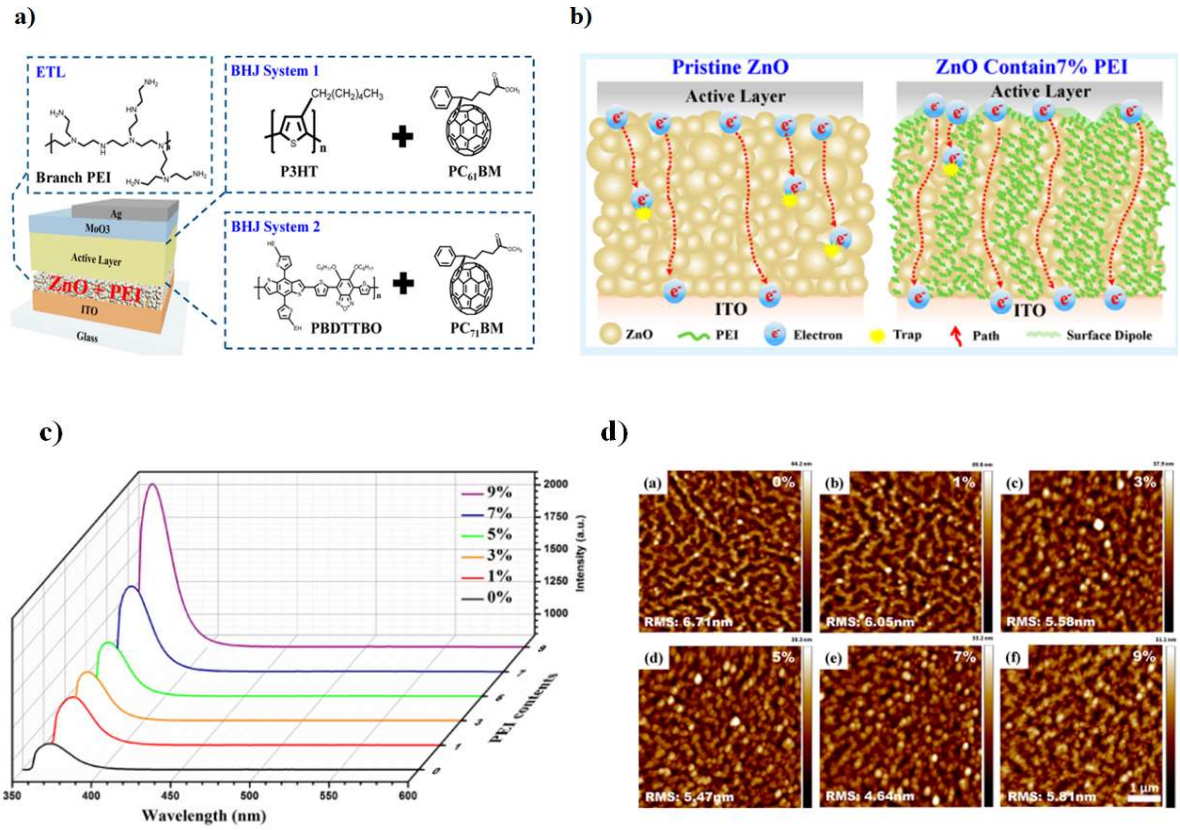

Figure 8. (a) Chemical structures of the compounds used to prepare BHJ solar cells (b) structural order of ZnO in the ZnO:PEI thin films align perpendicular to the ITO electrode (C) PL spectra of ZnO:PEI nanocomposite films incorporating PEI at various contents (0%, 1%, 3%, 5%, 7%, 9%) (d) AFM topographic images of ZnO:PEI blends films incorporating PEI at contents of (a) 0, (b) 1, (c) 3, (d) 5, (e) 7, and (f) 9 wt. % (H.-C. Chen et al., 2015).

There are numerous reports on Ni doped ZnO thin film deposition and characterization techniques, such as spin coating (Yildiz et al., 2011), sol-gel immersion (Ismail et al., 2018), magnetron sputtering, and spray pyrolysis (El Khalidi et al., 2019). In most situations, the electrical properties of Ni:ZnO thin films are found to be incompatible with Ni doping concentration, while optical parameters such as transmittance and band gap are incompatible with Ni doping. Rouchdi et al (Rouchdi, Salmani, el Hat, Mzerd, & Hassanain, 2016) disclose a controversial result in which the band gap of ZnO grows as Ni doping increases. Furthermore, M. Rouchdi, et al. (Rouchdi et al., 2016) report that the electrical conductivity of ZnO falls dramatically as Ni doping increases, which contradicts the concept of Ni doping. Because it is

logical to expect a decrease in resistivity with Ni replacing Zn as Ni is a good metal and a very minor mismatch of ionic radius between Zn^{2+} and Ni^{2+} ions generate low lattice distortion. Furthermore, Rajeh et al. (Rajeh et al., 2016) presented a disputed paper in which they claim that Ni-doping has no effect on the crystal growth plane of ZnO. However, elemental doping may modify the crystal habit plane for ZnO doped with (Cu, N), as observed by Liton et al. (Liton, Khan, Rahman, & Islam, 2015).

To summarize, despite multiple attempts to optimize the photovoltaic properties of P3HT: PC71BM-based organic solar cells utilizing ZnO ETLs doped with various metals, there is still a significant research area to utilize this material for OSCs employing Ni doping. Considering the wide range of uses for ZnO in optoelectronics, I am inspired to create ZnO and Ni doped ZnO thin films using a simple low-cost sol gel process. My goal is to investigate the influence of Ni doping on the structural, optical, and electrical characteristics of ZnO as an ETL for P3HT: PC71BM based organic solar cells. There have been no documented works using Ni ZnO ETL for P3HT: PC71BM blend active layer based solar cell, therefore this study contributes to understanding the impact of Ni at various concentrations on solar cell performance of P3HT based OSCs.

Table 1. Summary of the photovoltaic performance parameters for inverted organic Solar Cells using ZnO electron transport layers.

#	Device configuration	Jsc (mA/cm^2)	Voc (V)	FF (%)	PCE (%)	Ref.
1	ITO/ZnO/PM6:Y18/MoO3/Ag	25.71	0.84	84	15.7	(C. Zhu et al., 2020)
2.	ITO/ZnO/PBDBT:ITIC/MoO3/Ag	16.10	0.90	68.2	9.83	(Y. Wang et al., 2019)
3.	ITO/ZnO/PTB7Th:PC71BM/ MoO3/Al	16.88	0.80	68	9.18	(Y. Wang et al., 2018)
4.	ITO/ZnO/PTB7-Th:PC71BM MoO3/Ag	15.1	0.79	68.3	8.2	(Juang, Kao, Wang, Hsu, & Chen, 2018)

5	ITO/ZnO/C-QDs/PTB7: PC71BM/MoO3/Al	19.60	0.75	66.4	9.64	(Zhang et al., 2018)
6	ITO/ZnO-PAA/PBDTTPD:PC71BM/MoO3/Ag	12.1	0.86	54	5.6	(Eita et al., 2015)
7	ITO/ZnO-C60-EG/PTB7:PC71BM/MoO3/Ag	15.86	0.73	69.1	8.0	(T. Hu, Chen, Yuan, & Chen, 2015)
8	ITO/ZnO/C-PCBSD/ICBA:P3HT/PEDOT:PSS/Ag	12.4	0.84	60	6.22	(Stubhan et al., 2012)
9	ITO/ZnO-BisC60/PTB7-Th:PC71BM/MoO3/Ag	16.88	0.79	72.0	9.60	(S.-H. Liao et al., 2014)
10	ITO/ZnO-C60/PTB7-Th:PC71BM/MoO3/Ag	15.73	0.80	74.3	9.35	(S. H. Liao, Jhuo, Cheng, & Chen, 2013)
11	ITO/ZnO/P3HT:ICBA/MoOx/Ag	10.79	0.83	60	5.39	(Braid, 2016)
12	ITO/AZO/P3HT:PCBM/PEDOT:PSS/Ag	11.02	0.59	58.40	3.78	(S. Tsai et al., 2013)
13	ITO/ZnO:Mg/P3HT:PCBM/MoO3/Ag	9.7	0.58	56.8	3.17	(S. Tsai et al., 2013)
14	ITO/ZMO/PTB7:PC71BM/MoO3/Ag	16.78	0.74	66.99	8.31	(Yin et al., 2014)
15	ITO/ZnO/PCDTBT12:PC71BM/MoO3/Al	9.78	0.98	57.7	5.53	(Sun et al., 2012)
16	ITO/ZnO (SP)/P3HT:PCBM/WOx/Al	10.03	0.48	53	2.56	(Schumann et al., 2011)
17	ITO/ZnO / P3HT:PCBM/MoO3/ Ag	10.39	0.53	46.2	2.55	(X. Yu et al., 2013)

18	ITO/NZO/P3HT:PC71BM/MoO3/Al	13.6	0.57	48	3.72	Present work

CHAPTER THREE

3. Methods and Materials

3.1 Materials and Chemicals

The chemical precursors and materials, that were used in this thesis are: Zinc acetate dihydrate ($Zn(CH_3CO_2)_2 \cdot 2H_2O$, Energy Chemical, 99.5%), Nickel chloride hexahydrate ($NiCl_2.6H_2O$, Loba,98 %), poly (3- hexylthiophene) (P3HT, Sigma-Aldrich), [6,6]-phenyl-C_{71}-butyric acid methyl ester ($PC_{71}BM$, Sigma-Aldrich), 2-methoxyethanol($CH_3OCH_2CH_2OH$, Energy Chemical, 99%), Molybdenum Oxide (MoO_3, Sigma Aldrich) ethanolamine (CJ Chemicals, 99%), Ortho-dichlorobenzene (Chemical Co, 69%), Acetone (Dow Chemical, 99.5%), Ethanol (Loba Chemical, 99 %), Distilled water, ITO substrate, aluminum pellets, micropipettes, aluminum foil, beakers, magnetic stirrer, drying oven, hot plate, thermal evaporator, UV-ozone cleaner and solar simulator in addition to the usual characterization instruments mentioned above. All chemicals are used without any further purification unless otherwise stated.

3.2. Preparation of Pristine and Ni doped ZnO thin films

For the synthesis of undoped and Ni doped ZnO thin films, 1 M precursor solution was prepared by dissolving Zinc acetate dihydrate [$Zn(CH_3COO)_2 \cdot 2H_2O$] and Nickel chloride hexahydrate ($NiCl_2 \cdot 6H_2O$) in a mixture of 2-methoxyethanol (5 ml) and ethanolamine (0.1ml as a stabilizer). The solution was stirred overnight vigorously at room temperature in air. The ITO glass substrate was washed with soap and thoroughly cleaned using sequential ultrasonic treatments with, distilled water, acetone, and isopropanol for 20 min each. The cleaned ITO glass substrates were treated with UV-ozone cleaner for 20 min before depositing the ZnO films. Then the sol-gel processed pristine and Ni doped ZnO films were prepared by spin-coating the precursor solution twice onto the ITO substrates using a two-step spin coating process, at 1000 rpm for 10 s (first step) and at 2500 rpm for 30 s (second step). Then the films were annealed on the hot plate at 150 °C for 60 min in air, followed by cooling to room temperature before depositing the absorber layer as shown in Figure 9.

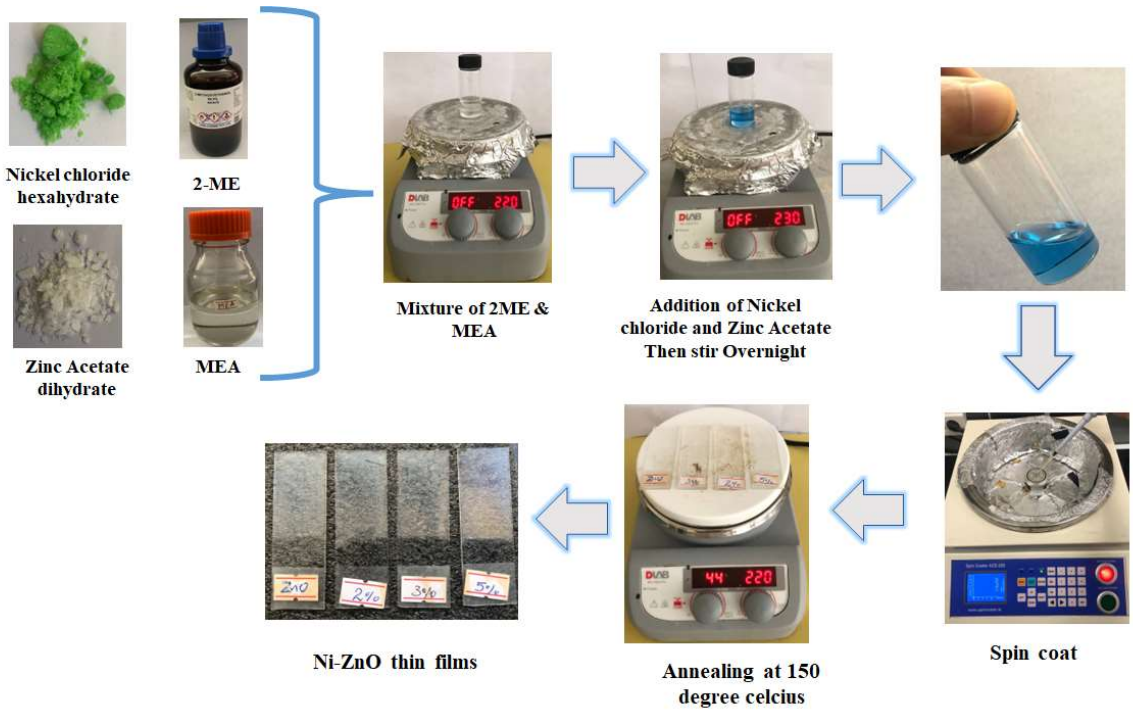

Figure 9. Preparation of Ni-ZnO thin films.

3.3. Solar cell device fabrication

The electron transport layers were deposited via spin-coating, on cleaned glass substrates, from solutions of ZnO with or without the inclusion of Ni. Solar absorber layer films were then spin-coated on the dried ETL layers from the solution of an active layer composed of P3HT: PC71BM blends at a 1:1 ratio. The active layer solution was prepared from P3HT and PC71BM polymers by blending a stoichiometric ratio of 1:1, in ortho-dichlorobenzene solvent at a 20 mg/ml concentration, after stirring for 4 hours at 60°C. The prepared solution was spun at 500 rpm for 10 s followed by 1000 rpm for 30 s. Then the film was annealed on the hot plate in the air at 130 ^{0}C for 10 min, followed by cooling to room temperature. Finally, to complete the device, a thin layer of MoO_3 as a hole transporting layer and Al as a hole collecting electrode were deposited continuously through thermal evaporation under a vacuum of ~5×10^{-6} Pa. The shadow mask was used during thermal evaporation to define the area of 0.04 cm^2. The schematic representation of the overall device fabrication process and device structure ITO/ZnO /P3HT: PC71BM/ MoO_3/Al are shown in Figure 10.

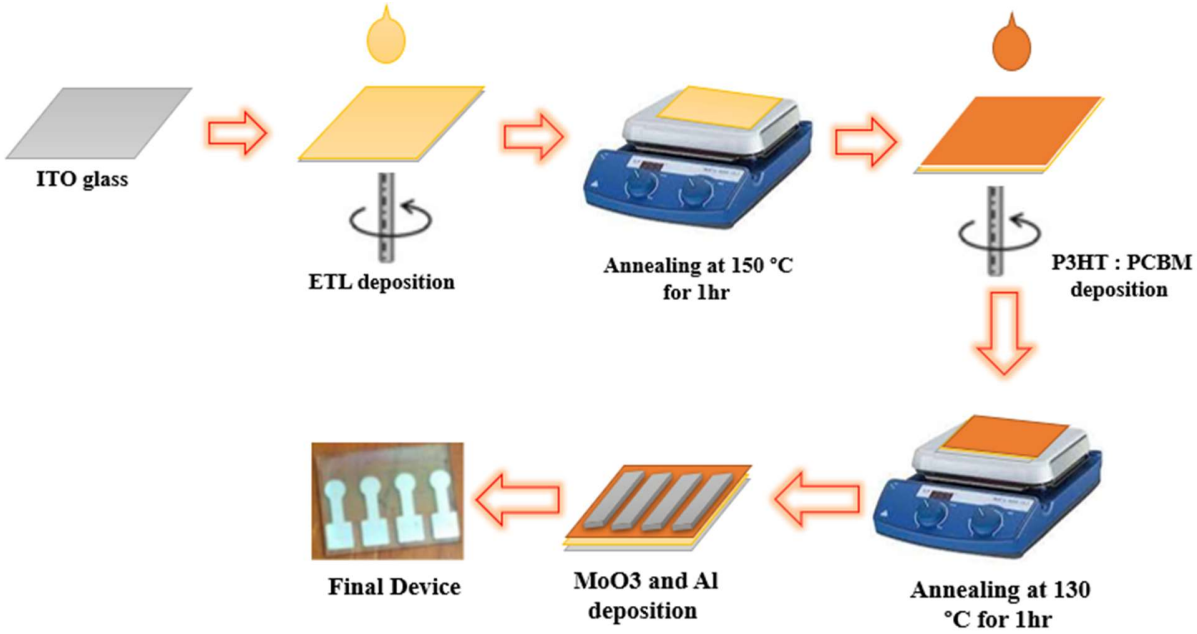

Figure 10. Overall schematic of fabrication of organic solar cells fabricated by one-step deposition method.

3.4. Material Characterizations

The morphology and crystal structure of the as-thin films are characterized by Scanning Electron Microscopy (SEM, JCM-6000Plus) and X-ray powder diffraction (Shimadzu XRD-7000) at copper Kα radiation (λCuKa=1.5418 Å), the scan speed of 3.000 (deg/min), voltage (40 kV), current (30mA) and scanning range ($10\text{-}80^0$) respectively. Absorption and photoluminescence (PL) spectra of the films prepared on glass were recorded using Perkin Elmer Lambda 19 UV-Vis/NIR spectrophotometer and HORIBA FLUROMAX- 4 spectrofluorometric, respectively. The J–V features of i-OSCs measurement were carried out under solar simulator operating at AM1.5 and integrated power intensity of 100 mW/cm^2 with computer interfaced Keithley HP2400 source-meter and a solar simulator (model SS50AAA).

CHAPTER FOUR

4. Result and Discussion

4.1. XRD analysis of pristine and Ni-doped Zinc Oxide films.

XRD analysis helps in the optimization of ETL manufacturing techniques by ensuring the desired crystal structure and composition are obtained. Figure 11 illustrates the XRD spectrum of Ni doped ZnO films. The intense and well-defined diffraction peaks for all films correspond to (100) and (101) planes which much very well with card No. (JSPDF File No. 89-1397). The XRD patterns also revealed that the films were in good crystallinity, the crystallites of the samples were oriented in two planes, and no impurities were found, indicating that Ni was successfully incorporated into ZnO without affecting its crystal structure. The dominant peak positions are observed at 2θ values of 31.94^0, on the other hand the minor peak observed at 56.77^0 corresponding to (100) and (101) planes respectively. Moreover, figure 11 indicates that the thin films are preferentially oriented along the two planes. In addition, as indicated by figure 11, the (100) and (101) plane of all Ni-ZnO films on the spectra showed a slight shift to the higher diffraction angle after Ni was introduced into the ZnO. This shift is explained by the substitutional replacement of bigger ionic radius Zn^{2+} (0.74 Å) with lower ionic radius Ni^{+2} (0.69Å).

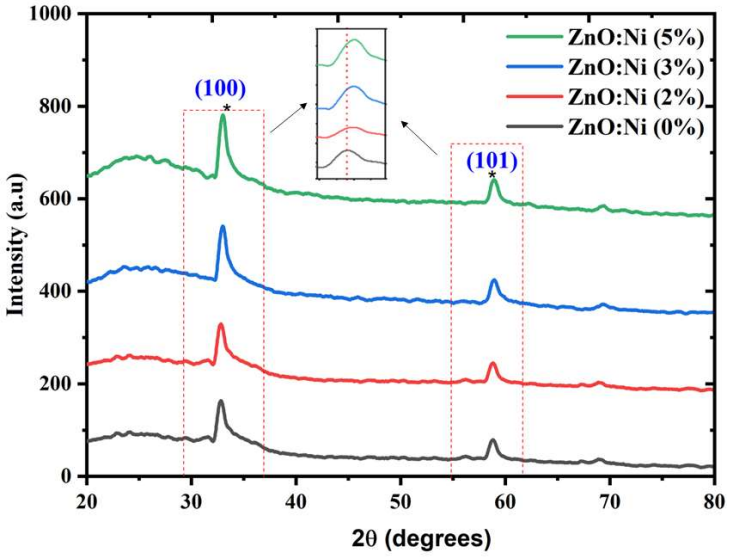

Figure 11. XRD pattern of pristine and Ni-ZnO thin films.

4.2. Optical properties of Ni-ZnO films.

The optical transmittance, absorbance and PL spectra of ZnO and Ni:ZnO thin films are shown in Figure 12. The UV-Vis absorption spectra of pristine and nickel doped ZnO films on glass are shown in Figure 12a. All doped and undoped films have optical absorption spectra that are only in the ultraviolet (UV) region, which is consistent with the transmission spectra. This is advantageous for preventing UV rays from reaching the active layer, since exposure to UV light may cause organic active layers to degrade (Bedia et al., 2014). A transmittance spectrum of ZnO thin films on glass without and with Ni concentrations of 2, 3, and 5 mol% is shown in Figure 12b. The ETL transports electrons from the light-absorbing layer to the electrode. It is intended to have higher transmittance because the greater the ETL transmittance, the lighter that reaches the light-absorbing layer and the more electrons that may be gathered for energy conversion, resulting in greater solar cell efficiency. The average transmittance (T_{ave}) of the thin films found to be 91.6, 90.3, 89.5 and 85.3 for ZnO, 2%, 3% and 5% by mole respectively. And it is clear that there is no substantial loss in transmission when Ni doping concentration is increased. The optical band gap values were determined from the optical absorption spectra using the Tauc relationship:

$$\alpha h\nu = A(h\nu - E_g)^n \qquad (3)$$

where $\boldsymbol{\alpha}$ is the absorption coefficient, hν is the photon energy, E_g is the band gap, A is a constant and n is 1/2 for allowed direct band gap. The value of exponent n depends upon the transition type, and it takes values 1/2, 2, 3/2 and three equivalents to the allowed direct, allowed indirect, forbidden direct and forbidden indirect transitions, respectively. The optical bandgap energies for all films with Ni concentrations of 0, 2, 3, and 5 % by mole were 3.38 eV, 3.36 eV, 3.35 eV and 3.28 eV respectively. When Ni doping is increased, a red shift at the band edge absorption is seen, indicating that the band gap was reduced as a result of the increased Ni doping. The reduction in the band gap energy can be explained by the sp-d exchange interaction, in which s p and d orbitals are involved in the formation of covalent bonds in ZnO structure, and their hybridization determines the electronic properties of ZnO. The valence band (VB) of pure ZnO is mostly composed of deep Zn 3d states and O 2p states. There is significant repulsion between these states, which stabilizes the VB (Das et al., 2013). As illustrated in figure 12d, Ni doping introduces the shallower, occupied Ni 3d states, which mix strongly with the O 2p states (unlike

the Zn 3d states), widening the overall VB and pushing VB_{max} up in energy, hence lowering the band gap (H Ali et al., 2020; M. Y. Ali et al., 2020; Das et al., 2013; Kamruzzaman, Luna, Podder, & Anowar, 2012).

Photoluminescence spectroscopy is extremely useful for investigating the presence of various intrinsic defects in pristine and doped ZnO films by determining various radiative recombination's and trapping levels. Figure 12c depicts the variation in photoluminescence intensity with wavelength for ZnO and Ni:ZnO thin films at an excitation wavelength of 280 nm. The room temperature photoluminescence (RTPL) spectra were taken in the wavelength range of 320 nm–500 nm. The PL peaks of the ZnO and Ni:ZnO samples are almost in the same position but have different intensities, as can be seen in the Figure 12c. According to the figure, the blue emissions were produced by the recombination of trapped holes and electrons at Zn vacancies (V_{Zn}) and Zn interstitial (Zn_i), respectively, as well as the recombination of trapped electrons at Zn_i sites with photo-generated holes (H Ali et al., 2020). V_{Zn} and Zn_i are predicted to form more easily within ZnO matrices due to their lower formation energy (Kavitha, Jinesh, Philip, Gopinath, & John, 2014). The intensity of the UV emission band around 345 nm is determined by band-to-band transitions, which are caused by photogenerated electron and hole recombination in the conduction and valence bands, respectively. In ZnO, the O_i and V_{Zn} energy levels are closer to the valance band (VB), whereas the Zn_i and V_O levels are closer to the conduction band (CB) (Jadhav & Biswas, 2016). The emission bands observed at 425 and 455 nm may be caused by an electron transition from the Zn_i site's energy level to the top of the valance band (VB) of ZnO (Farag, Cavaş, Yakuphanoglu, & Amanullah, 2011). The peak at 475 nm, on the other hand, is caused by electron transitions between the bottom of the conduction band (CB) and the acceptor V_{Zn} site (H. Ali et al., 2020). The peak at 493 nm is originated due to defects caused by oxygen i.e. oxygen vacancy or oxygen interstitial (Bomila, Srinivasan, Venkatesan, Bharath, & Perinbam, 2018). It's clear from the graph that radiative recombination is enhanced meaning that the Ni:ZnO films have good quality or less defects as compared to the pristine ZnO thin film. Radiative recombination is desired because it improves the process of photon recycling, in which photons emitted by recombining charges in the ETL are trapped and reabsorbed by the active layer leading to additional excitations and thus contributing to an increase in photocurrent (Fell et al., 2021). In solar cell, a photon from sunlight enters and is absorbed by the semiconductor material, exciting an electron from the

valence band to the conduction band. If that excited electron recombines with defects or impurities and the energy that was absorbed is lost as heat, leading to a reduction in the PL spectrum. However, if the excited electron recombines with a hole in the valence band while emitting a photon, then the energy is released as light, some of which is trapped within the solar cell, increasing the chance that the energy will be absorbed again and converted into electrical energy.

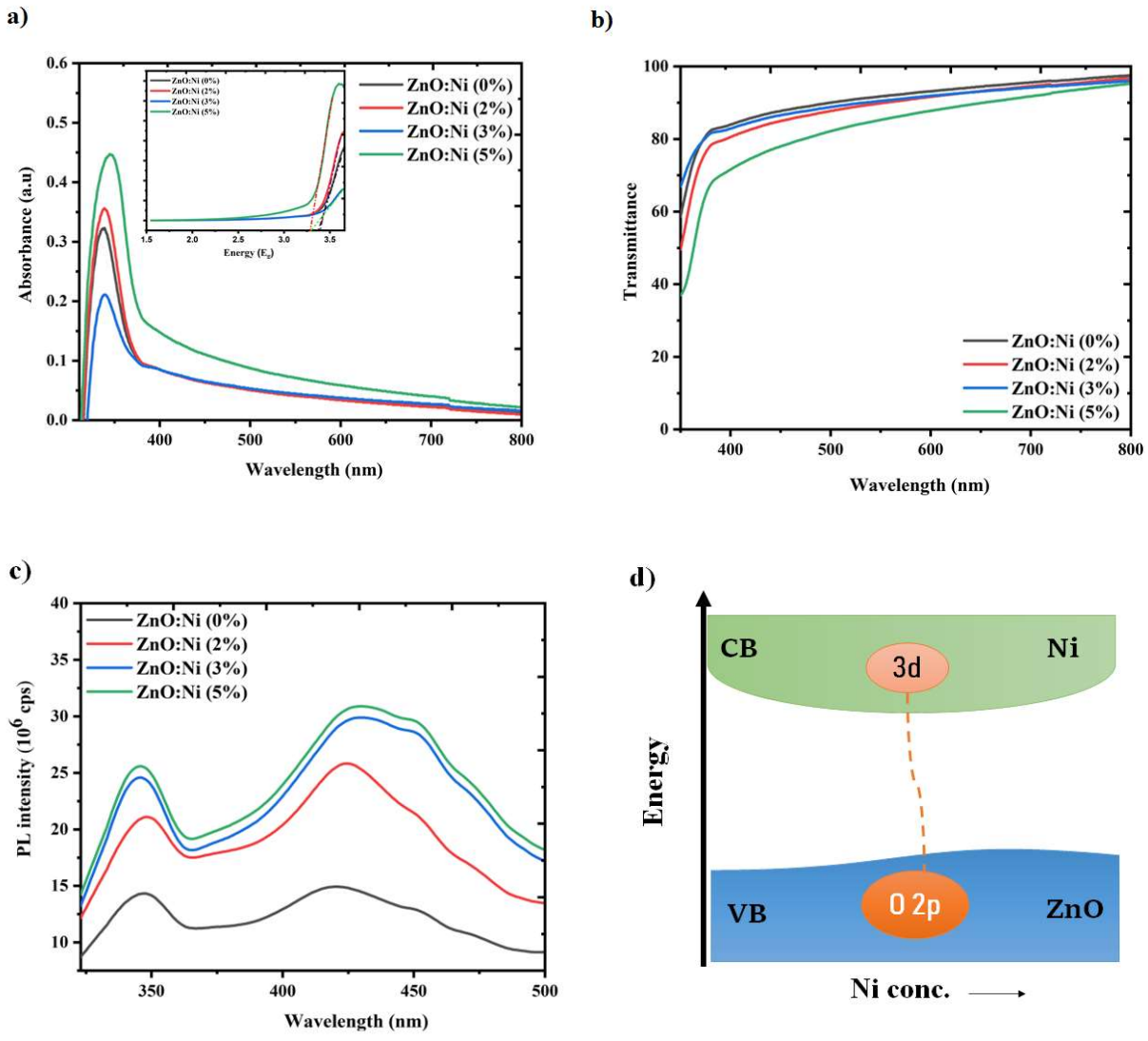

Figure 12. (a) Absorption (inset is tauc plots), (b) transmittance and (c) PL spectra of thin films with structure glass/ZnO with pristine ZnO and ZnO doped with different concentration of Ni. d) band gap tuning through nickel doping.

4.3. Morphology of the pristine and Ni-ZnO ETL films

The morphology of ETL is known to play a critical role in transporting photogenerated current to the respective electrode, which ultimately affect the performance of solar cell device. Figure 13 shows the surface morphologies of the deposited films taken by SEM at 1500× magnification. The film surfaces were discovered to evenly cover the substrates. The SEM pictures revealed that the deposition resulted in clusters with well-defined clusters made up of highly dense ganglia-like fibers spread across a large area. Such ZnO and Ni:ZnO nanofiber growth have also been reported (M. Y. Ali et al., 2020; Das et al., 2013). From structures seen in each case, it is clear that ZnO structure is getting smoother and smoother indicating reduced imperfections that can impede the flow of electrons through the material, allowing easier charge flow, resulting in increased conductivity of the ETLs. This could also help us to understand the improved FF for 2% and 3 mol% devices (see table 3). Nonetheless, at 5% nickel doping, as indicated in figure 13, agglomerated domains began to form. Which in the long run, affect the active layer-ETL interface.

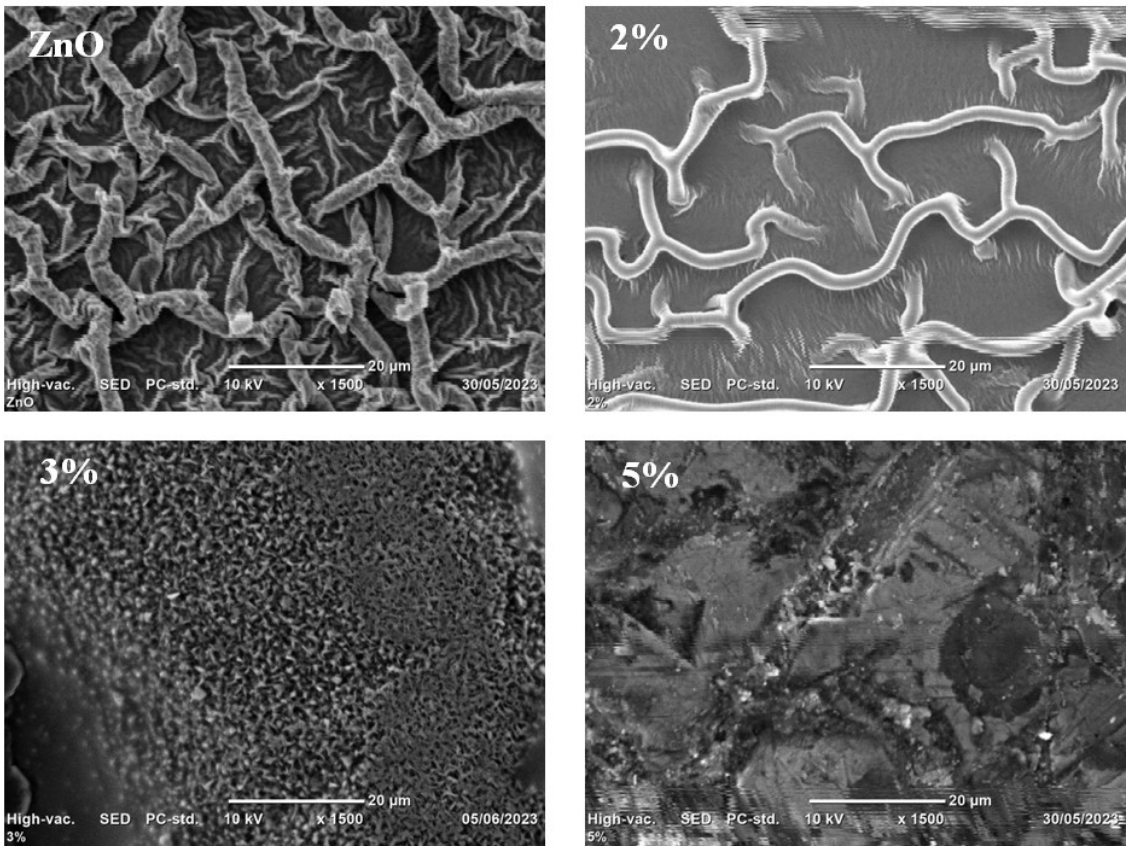

Figure 13. SEM micrographs at magnification of 1500X for pristine and Ni-ZnO thin films.

4.3. Electrical properties of pristine and Ni-ZnO ETL

The free charge collection of the OSC devices is determined by the electrical conductivity the ETL. The conductivities of the pristine and Ni doped ZnO films were estimated from the slope of their IV characteristics using equation (4) (Choi et al., 2018) with geometry ITO/ZnO:Ni/Al under dark condition.

$$\sigma = G \times L/A \qquad (4)$$

Where σ is the electrical conductivity, G is the conductance (slope on the I-V curve), L is the thickness of the film (40 nm) and A is the active area (0.04 cm^2).

Figure 14b presents the obtained electrical conductivity plot against the dopant concentration and the values of conductivity were summarized in Table 1. As indicated in Figure, the undoped device exhibited less ohmic behavior and conductivity whereas the ohmic and conductivity

behavior of the Ni-doped device were significantly improved. The increase in the electrical conductivity is due to the introduction of nickel ions into zinc oxide lattice, Zinc has a full 3d shell of electrons in its valence band, which means that it does not contribute many free electrons to conduction in the material. However, when Ni is substituted for some of the Zn atoms, it brings with it a partially-filled 3d shell (with 8 electrons) that lies near the bottom of the conduction band. These additional conduction band states allow more electrons to contribute to current flow, increasing the material's conductivity (M. Y. Ali et al., 2020; Kamruzzaman et al., 2012). This one order improvement in electrical conductivity of the Ni doped ZnO layer over the pure ZnO layer is anticipated due to the films' enhanced morphology (see figure 13), which lowers recombination losses during charge collection.

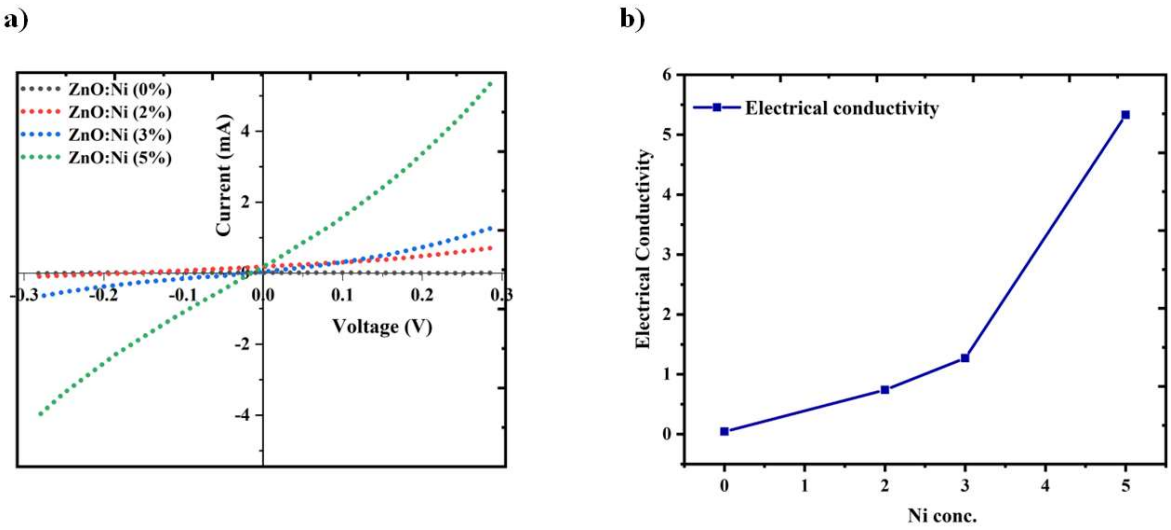

Figure 14. Plot showing the I-V curve (a) and calculated electrical conductivity of thin films with structure ITO/ZnO/Al with pristine ZnO and ZnO doped with different concentrations of Ni (b).

Table 2 Electrical conductivity of ITO/Ni-ZnO /Al thin films with different concentrations of Ni.

Ni concentration	Conductivity(s/m)
0	4.48×10^{-5}
2	7.39×10^{-5}

3	1.27×10^{-4}
5	5.33×10^{-4}

4.4. Optical properties of the active layer

Figure 15 depicts the UV-Vis absorption spectra of ZnO/ P3HT: PC71BM films on glass without and with various Ni doping concentrations. This is to better understand the impact of Ni doping on ZnO on photon harvesting in the OSCs' active layer. The active layer coated on ZnO doped with 3 mol.% Ni exhibits the maximum absorption, indicating a superior photon harvest and stronger photogeneration. This might be attributed to the film's and active layer better aggregation (J.-H. Tsai et al., 2010). However, the 5% Ni-ZnO's poor interface with the active layer (see figure 13) consequently led to low absorption of light by the active layer. Aside from that, the absorption spectra indicated no ZnO-related absorption peak, showing that the ZnO layer has the maximum light transmission.

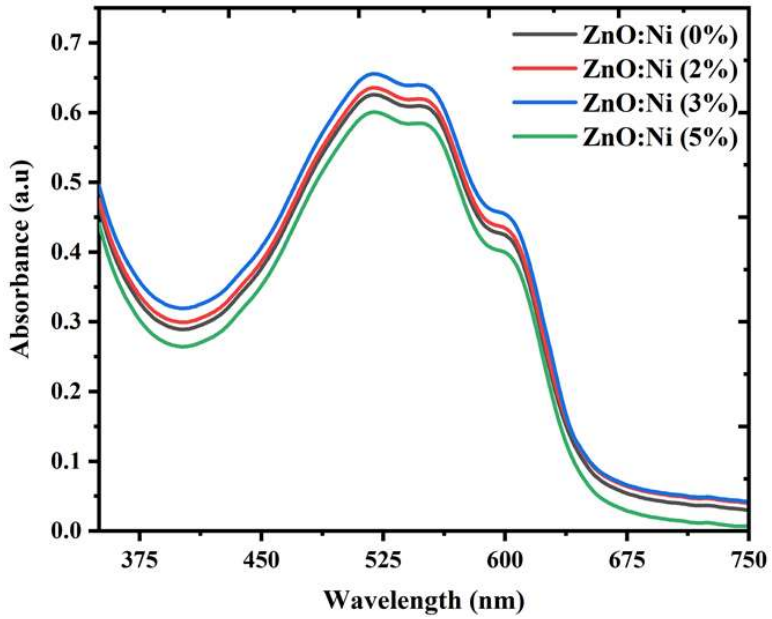

Figure 15 . Plot showing absorbance of the film with structure Glass/ZnO/P3HT: PC71BM with pristine ZnO and Ni- ZnO ETL.

4.5. Photovoltaic Properties

To explore the influence of Ni-doping of ZnO ETL on device performance of bulk heterojunction OSCs were built in an inverted configuration as shown in figure 16c. Figure 16 (a) and (b) show the current density-voltage (J-V) characteristics of the constructed device under the illumination of an AM 1.5 solar simulator at a light intensity of 100 mW/cm^2 and in the dark respectively. The device with 3 mol.% Ni dopants has the maximum power conversion efficiency (PCE) of 3.72%, which is 50% greater than the pure ZnO (2.48%). Furthermore, the short-circuit current density (J_{sc}) is increased by 40% and the fill factor (FF) by 14%. Table 3 summarizes the solar cell characteristics for the devices, including open-circuit voltage (V_{oc}), Jsc, FF, PCE, series resistance (R_s), and shunt resistance (R_{sh}). The introduction of Ni in the ZnO layer results in a significant improvement in PCE, which is beneficial to optimising charge dissociation, charge mobility, and collecting processes. The open-circuit voltage (V_{oc}) doesn't change significantly, but the short-circuit current (J_{sc}) is quite enhanced. This can occur when there is a rise in light absorption in the device's active layer, resulting in more excitons being created and, as a result, more charge carriers being collected. This can result in an increase in J_{sc} without modifying the device's voltage characteristics. However, it is crucial to remember that other elements, such as the fill factor, which is connected to the device's internal resistance, influence the total efficiency of the device, and they should be considered when evaluating the performance of organic solar cells.

The device's performance exhibited significant enhancements when the Ni content was gradually increased to 3 wt.%. This improvement can be credited to multiple factors, including the increased electrical conductivity of the ETL and improved absorption of the active layer, as depicted in Figure 15**.** These advancements ultimately led to better photocurrent generation and charge collection. It is worth mentioning that the rise in FF is due to enhanced charge mobility (see table 5) and decreased series resistance (R_s). Despite having high electrical conductivity, the ZnO electron transport layer (ETL) with 5 mol% Ni exhibits the lowest power conversion efficiency (PCE) of 1.48. There are multiple factors that contribute to this outcome. One of the reasons is the higher series resistance (R_s) present in the device, which hinders the movement of free charge carriers after dissociation. This limits charge mobility within the device, as evident in table 5, ultimately leads to a decrease in the overall power conversion efficiency (PCE) value. Furthermore, the lower shunt resistance of the device suggests the presence of

higher leakage current, as shown in Figure 16. This indicates the occurrence of electrical losses within the device, meaning that some of the electrical charge generated by the device is lost due to high resistance or defects in the device materials. Furthermore, the device exhibits enhanced charge carrier recombination rates, as evidenced by the PL plot (see Figure 17b). As a result, charge carrier dissociation at the polymer blend interface is minimized, resulting in lower charge mobility and PCE value.

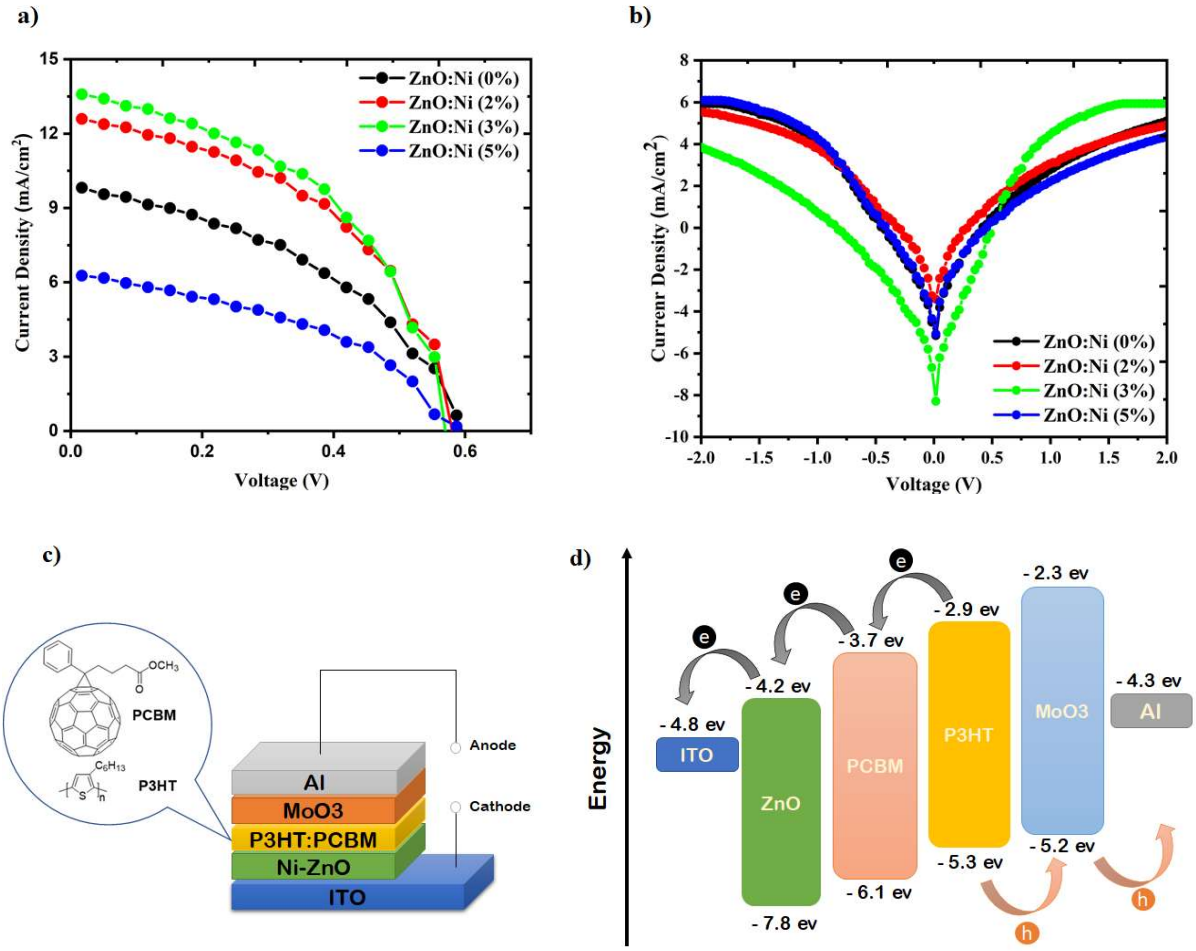

Figure 16. J-V characteristics of solar cells with structure ITO/ZnO/P3HT: PC71BM/MoO3/Al where ZnO is incorporated with different Ni concentration under illumination (a), under dark (b), (c) The device architecture of inverted OSCs with Ni-ZnO ETL d) Energy level diagram of the fabricated devices.

Table.3 Summary of device performance for solar cell structure with ITO/ZnO (with different concentrations of Ni)/P3HT: PC71BM/MoO_3/Al.

Ni conc.	Voc	Jsc ($mAcm^{-2}$)	FF	PCE (%)	Rs	Rsh
0	0.59	9.7	42	2.4	293.1	2872.8
2	0.58	12.6	47	3.47	204.7	3959.1
3	0.57	13.6	48	3.72	174.4	4779.9
5	0.57	6.2	42	1.48	499.8	2839.4

From figure 16b, it was observed that the J-V curves of Ni-ZnO ETL devices, except for the 5 mol% doping concentration, showed reduced reverse saturation current (also known as leakage current) compared to devices with only ZnO ETL. This finding aligns with the R_{sh} (shunt resistance) values mentioned in table 3. Additionally, the devices with 2 and 3 mol % Ni doping displayed enhanced forward output current (which agrees with lower R_s value in table 3). These results indicate that the introduction of Ni doping improves both the charge selectivity and charge transport ability of the ZnO ETL, Since the magnitude of the forward bias current is directly related to the charge carrier generation and transport properties of the device, including the mobility of the charge carriers, and the recombination rate (X. Song et al., 2021). Meanwhile, A smaller leakage current indicates that the solar cell device converts light more efficiently. This is due to the fact that the leakage current measures the amount of current that passes through the cell while no light is shining on it (X. Yu et al., 2014), which greatly altered charge transport and extraction. However, 5 mol% Ni-doped ZnO ETL showed larger leakage current and lower forward bias current, which aligned with the series resistance (R_s) and shunt resistance (R_{sh}) values provided in Table 3. This finding is the consequence of greater recombination of photogenerated charge carriers after dissociation, resulting in a lower fill factor (FF) value, as seen in Table 3. Obviously, the Ni-doping improves the overall photovoltaic performance of Ni-ZnO devices, and there is an obvious charge transfer improvement.

4.6. Study of charge generation and exciton dissociation

Exciton dissociation and charge generation of pristine and nickel doped Zinc oxide was investigated to better understand the rationale for PCE improvement. Upon photon absorption, the exciton created in the active layer should dissociate into free charges to generate photocurrent in OSC. The device PCE depends on both exciton dissociation and charge creation. Figure 17a exhibits, the photo-current density given by, $J_{ph}= J_L - J_D$ (where J_L and J_D indicate the current density under illumination and in the dark, respectively), and it's dependent on the effective applied voltage, $V_{eff} =V_o - V_a$ (where V_a is the applied voltage and V_o is the voltage at which $J_{ph} = 0$) (Luo et al., 2019). It's clearly from the figure, J_{ph} rises linearly with effective voltage first before saturating at J_{sat}. The applied electric field, however, is insufficient to sweep out all charge carriers in the linearly rising area of J_{ph} Vs V_{eff}. Further increase in the electric field will dissociate all of the excitons and current is collected. Figure 17a demonstrates that J_{ph} rose with V_{eff} in the low effective voltage range, showing that the photocarriers dissociate into free charges, which are finally collected at their corresponding electrodes. Enhanced carrier transport directly correlates with an increase in the maximum exciton generation rate (G_{max}), i.e., $J_{sat} = qLG_{max}$, where q and L indicate the electronic charge and active layer thickness (100 nm), respectively (J. Li et al., 2018). As summarized in table 3, the G_{max} is significantly enhanced after incorporating 3mol% Ni in ZnO ETLs, from 9.77 x 10^{21} s^{-1} cm^{-3} of pure ZnO to 11.93 x 10^{21} s^{-1} cm^{-3} of 3 mol% Ni-ZnO ETL. Since G_{max} is proportional to the maximum number of photons absorbed, it is demonstrated that almost all of the photoinduced holes and electrons of 3mol% Ni-ZnO devices are transported into the individual electrodes, and the probability of generating recombination becomes very small in the saturation region (J. Li et al., 2019). However, the device with a 5 mol% Ni-ZnO ETL demonstrated a decreased G_{max} as a result of the low absorbance of incoming light by the absorber layer. This phenomenon can potentially be attributed to the inadequate interaction at the interface between the ETL and the active layer, which is in agreement with the SEM micrograph in Figure 13.

According to Figure 17, the rate of exciton formation rises in a linear fashion as the nickel content increases, which can be attributed to an increase in the absorbance of the active layer. However, when the Nickel concentration reaches 5 mol%, the exciton formation rate decreases due to the insufficient absorbance of the active layer. As a result, charge carriers are generated

in the active layer, and then they move through the material to their respective electrodes for charge collection. Exciton quenching efficiency was also calculated in order to better understand the rationale for the PCE enhancement using equation (5) (Tegegne, 2018).

$$QE\ (\%) = \left(1 - \frac{PL_{blend}}{PL_{polymer}}\right) \times 100 \qquad (5)$$

, where PL_{blend} and $PL_{polymer}$ correspond to the PL recorded in the P3HT: PC71BM/ETL/Glass and the P3HT/Glass, respectively.

Exciton quenching efficiency (QE) of active layers coated on pristine and Ni doped ZnO ETLs was examined to further understand the rationale for PCE enhancement, as shown in figure 17b. PL spectra of P3HT: PC71BM coated on Ni-doped and undoped ZnO ETL films were recorded at room temperature using a 520 nm excitation wavelength. The PL intensity of the P3HT-only film was much higher due to maximum exciton recombination caused by the lack of an exciton dissociation route. When P3HT was blended with PC71BM, the PL of P3HT was suppressed due to exciton dissociation at the donor/acceptor interface. Similarly, the PL of the active layer coated on the ETL was quenched with increasing nickel concentration (with the lowest value observed at a 3 mol% doping level) due to exciton dissociation at the donor/acceptor interface. After exciton dissociation, the electron in the PC71BM moves towards the ETL, reducing the likelihood of recombination and consequently leading to a decrease in PL intensity, as illustrated in Figure 17b.

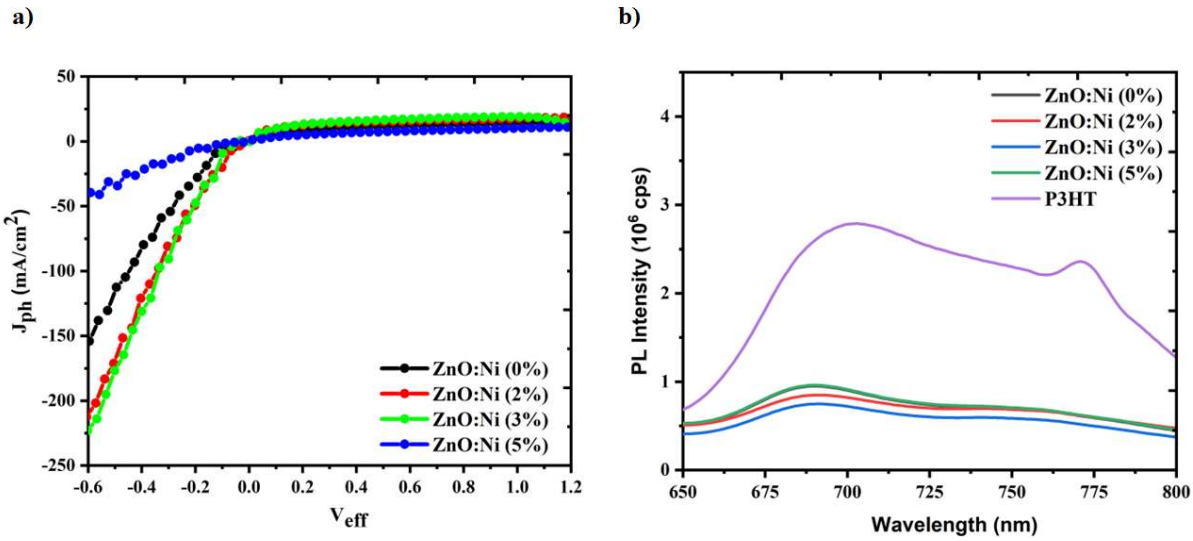

Figure 17. J_{ph} vs V_{eff} curves (a) and Exciton Quenching (b) in OSC prepared with pristine ZnO and Ni-ZnO ETL.

Table 4 J_{sat} and G_{max} of OSC under short-circuit condition with various concentration of Ni.

Ni conc. (mol. %)	QE (%)	J_{sat} (mA/cm^2)	G_{max} (s^{-1} cm^{-3})x10^{21}
0	65.5	15.6	9.7
2	69.1	17.3	10.8
3	72.5	19.1	11.9
5	64.8	9.6	6.01

4.7. Charge mobility Measurement

To investigate the impact of Ni doping on the electron mobilities of manufactured devices, electron alone devices with geometry, ITO/Ni:ZnO/Al with pristine and various nickel dopant concentrations were prepared, and the corresponding electron mobility was calculated using the Motto-Gurney space charge limited current (SCLC) given in equation 6 (Hamed, Ike, & Mola, 2021) as:

$$J_{SCLC} = \frac{9}{8}\mu_e\,\varepsilon_o\varepsilon_r\frac{V^2}{L^3} \qquad (6)$$

Where, μ_e, ε_o, ε_r, V and L the electron mobility, vacuum dielectric constant (ε_o=8.95x10^{-12} F/m), the dielectric constant of P3HT: PC71BM (ε_r=3) (B. Han et al., 2014), the applied voltage and the thickness of the absorber layer (100 nm), respectively. The extracted electron mobility of an electron-only device was 6.91 x 10^{-5} cm^{2}S^{-1}V^{-1}, 8.03 x 10^{-5} cm^{2}S^{-1}V^{-1}, 8.14 x 10^{-5} cm^{2}S^{-1}V^{-1} and 4.69 x 10^{-5} cm^{2}S^{-1}V^{-} for devices made from ETL doped Ni with 0, 2, 3, and 5 mol% respectively.

Table 4 clearly indicates that the inclusion of the Ni dopant in the electron transport layer (ETL) significantly enhanced electron mobility. Among the different devices tested, the one based on a 3 mol% Ni-ZnO ETL concentration demonstrated the highest electron mobility. This conclusion is supported by lower series resistance (R_s) and a higher fill factor (FF), indicating a lower rate of recombination in the device. Additionally, the device with 3 mol% Ni showed increased absorption in the active layer, as depicted in Figure 15. Moreover, it exhibited reduced

exciton recombination and improved exciton dissociation, as illustrated in Figure 17a. On the other hand, the device with 5 mol% Ni exhibited the lowest electron mobility, evidenced by lower absorption of the active layer and a higher Rs. This outcome can be attributed to higher exciton recombination and lower exciton dissociation, which are depicted in Figure 17d.

Table 5. Electron mobility of pristine and Ni doped ZnO ETL devices

Ni conc. (mol. %)	μ_e ($cm^2S^{-1}V^{-1}$)
0	6.91×10^{-5}
2	8.03×10^{-5}
3	8.14×10^{-5}
5	4.69×10^{-5}

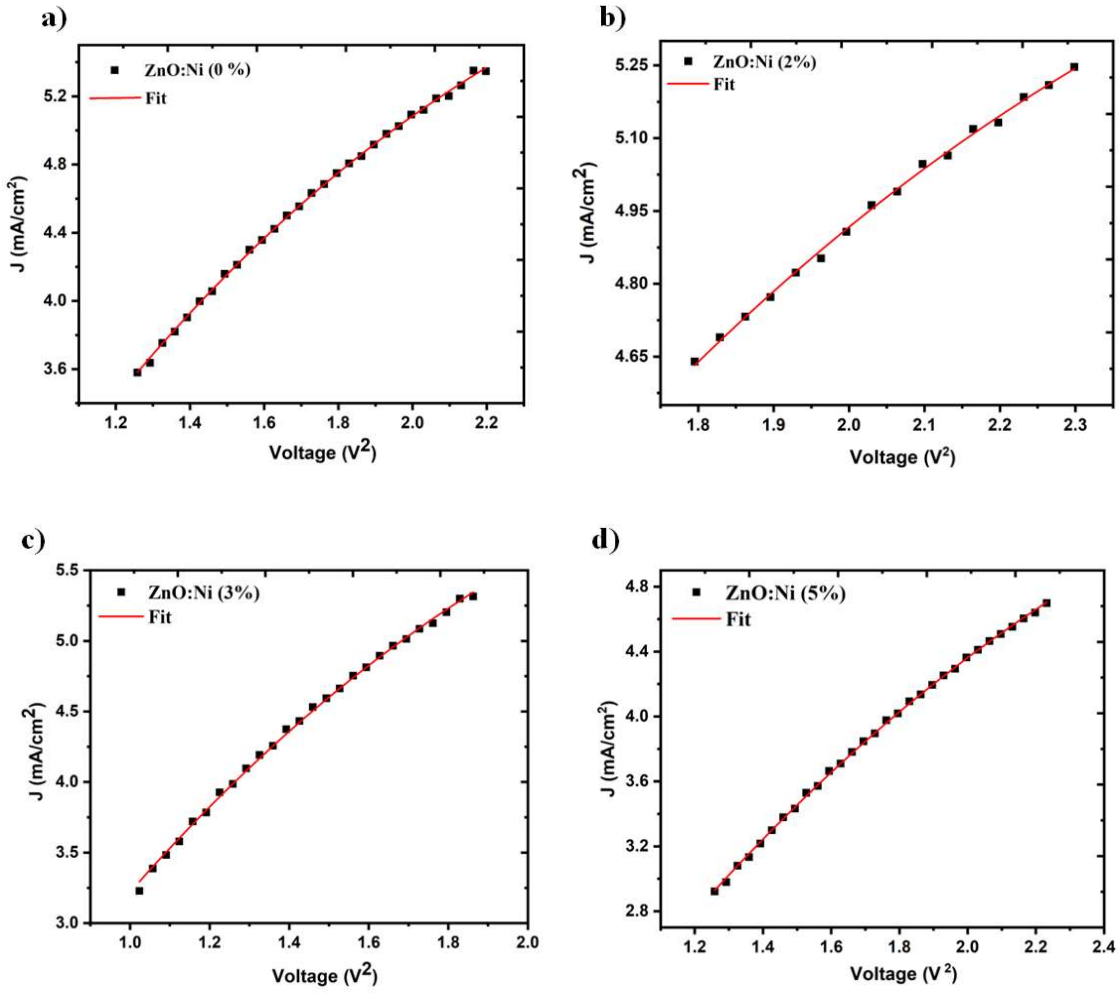

Figure 18. Electron mobility of devices a) pristine ZnO b) 2% Ni doped c) 3% Ni doped and d) 5% Ni doped ZnO ETLs

Conclusion

To sum up, room temperature sol-gel process was used to prepare pristine and Ni-doped ZnO films as electron transport layers for i-OSCs. The Ni-ZnO films were characterized by XRD, UV-Vis spectrophotometer, PL and IV. Improved optical, electrical and structural results were obtained upon nickel doping. When compared to undoped ETL device, the constructed solar cell devices made from Ni-doped ETL (except for 5mol%) exhibited a significant improvement in device performance, namely better solar cell parameters such as short-circuit current densities (J_{sc}), series resistance, and fill factor (FF). This improved device performance attributed to increased electrical conductivity, enhanced absorption of light by the active layer and lower recombination of the photogenerated charge carriers within the device. Furthermore, charge generation and electron mobility measurements were taken and found out consistent with the performance of the devices. As a result, our findings demonstrate that Ni-ZnO is a promising electron transport layer for OSCs.

Recommendations

The breadth of this work is limited by time, work environment, and financial factors. Based on the findings, several recommendations for further work can be made. The as-prepared Ni-ZnO ETL showed promise for improving the performance of OSCs. However, in order to perform a complete inquiry into the possible use of these intriguing materials as ETL for OSCs, I strongly suggest that the study be conducted in a pleasant environment with suitable facilities and characterization instruments. I also advocate for more research into the possible use of these materials as ETL for other polymers and inorganic-based solar cells.

References

Abdulrazzaq, O. A., Saini, V., Bourdo, S., Dervishi, E., & Biris, A. S. (2013). Organic Solar Cells: A Review of Materials, Limitations, and Possibilities for Improvement. *Particulate Science and Technology, 31*(5), 427-442. doi:10.1080/02726351.2013.769470

Ali, H., Alsmadi, A., Salameh, B., Mathai, M., Shatnawi, M., Hadia, N., & Ibrahim, E. (2020). Influence of nickel doping on the energy band gap, luminescence, and magnetic order of spray deposited nanostructured ZnO thin films. *Journal of Alloys and Compounds, 816*, 152538.

Ali, H., Alsmadi, A. M., Salameh, B., Mathai, M., Shatnawi, M., Hadia, N. M. A., & Ibrahim, E. M. M. (2020). Influence of nickel doping on the energy band gap, luminescence, and magnetic order of spray deposited nanostructured ZnO thin films. *Journal of Alloys and Compounds, 816*, 152538. doi:https://doi.org/10.1016/j.jallcom.2019.152538

Ali, M. Y., Khan, M., Karim, A. T., Rahman, M. M., & Kamruzzaman, M. (2020). Effect of Ni doping on structure, morphology and opto-transport properties of spray pyrolised ZnO nano-fiber. *Heliyon, 6*(3), e03588.

Alstrup, J., Jørgensen, M., Medford, A. J., & Krebs, F. C. (2010). Ultra fast and parsimonious materials screening for polymer solar cells using differentially pumped slot-die coating. *ACS applied materials & interfaces, 2*(10), 2819-2827.

Ambade, R. B., Ambade, S. B., Mane, R. S., & Lee, S.-H. (2015). Interfacial engineering importance of bilayered ZnO cathode buffer on the photovoltaic performance of inverted organic solar cells. *ACS applied materials & interfaces, 7*(15), 7951-7960.

Atesin, T. A., Bashir, S., & Liu, J. L. (2017). *Nanostructured Materials for Next-Generation Energy Storage and Conversion*: Springer.

Bedia, F. Z., Bedia, A., Maloufi, N., Aillerie, M., Genty, F., & Benyoucef, B. (2014). Effect of tin doping on optical properties of nanostructured ZnO thin films grown by spray pyrolysis technique. *Journal of alloys and compounds, 616*, 312-318.

Bolognesi, M. (2013). *Organic bulk-heterojunction photovoltaic devices: materials, device architectures and interfacial processes.* Universitat Rovira i Virgili,

Bomila, R., Srinivasan, S., Venkatesan, A., Bharath, B., & Perinbam, K. (2018). Structural, optical and antibacterial activity studies of Ce-doped ZnO nanoparticles prepared by wet-chemical method. *Materials Research Innovations, 22*(7), 379-386.

Braid, J. L. (2016). *Understanding efficiency improvement in organic photovoltaics with molecular modifiers*: Colorado School of Mines.

Carter, S., Angelopoulos, M., Karg, S., Brock, P., & Scott, J. (1997). Polymeric anodes for improved polymer light-emitting diode performance. *Applied physics letters, 70*(16), 2067-2069.

Chambon, S., Derue, L., Lahaye, M., Pavageau, B., Hirsch, L., & Wantz, G. (2012). MoO3 thickness, thermal annealing and solvent annealing effects on inverted and direct polymer photovoltaic solar cells. *Materials, 5*(12), 2521-2536.

Chen, H.-C., Lin, S.-W., Jiang, J.-M., Su, Y.-W., & Wei, K.-H. (2015). Solution-processed zinc oxide/polyethylenimine nanocomposites as tunable electron transport layers for highly efficient bulk heterojunction polymer solar cells. *ACS applied materials & interfaces, 7*(11), 6273-6281.

Chen, L. M., Hong, Z., Li, G., & Yang, Y. (2009). Recent progress in polymer solar cells: manipulation of polymer: fullerene morphology and the formation of efficient inverted polymer solar cells. *Advanced Materials, 21*(14-15), 1434-1449.

Choi, J., Jo, J. W., de Arquer, F. P. G., Zhao, Y. B., Sun, B., Kim, J., . . . Seifitokaldani, A. (2018). Activated Electron-Transport Layers for Infrared Quantum Dot Optoelectronics. *Advanced Materials, 30*(29), 1801720.

Chueh, C.-C., Li, C.-Z., & Jen, A. K.-Y. (2015). Recent progress and perspective in solution-processed Interfacial materials for efficient and stable polymer and organometal perovskite solar cells. *Energy & Environmental Science, 8*(4), 1160-1189.

Das, S. C., Green, R. J., Podder, J., Regier, T. Z., Chang, G. S., & Moewes, A. (2013). Band Gap Tuning in ZnO Through Ni Doping via Spray Pyrolysis. *The Journal of Physical Chemistry C, 117*(24), 12745-12753. doi:10.1021/jp3126329

Duan, L., & Uddin, A. (2020). Progress in stability of organic solar cells. *Advanced Science, 7*(11), 1903259.

Eita, M., Labban, A. E., Cruciani, F., Usman, A., Beaujuge, P. M., & Mohammed, O. F. (2015). Ambient Layer-by-Layer Zno Assembly for Highly Efficient Polymer Bulk Heterojunction Solar Cells. *Advanced Functional Materials, 25*(10), 1558-1564.

El Khalidi, Z., Hartiti, B., Siadat, M., Comini, E., Arachchige, H. M. M., Fadili, S., & Thevenin, P. (2019). Acetone sensor based on Ni doped ZnO nanostructues: growth and sensing capability. *Journal of Materials Science: Materials in Electronics, 30*, 7681-7690.

Eshete, Z. S., Mulatu, D. W., & Gatiso, T. G. (2020). CO2 emissions, agricultural productivity and welfare in Ethiopia. *International Journal of Climate Change Strategies and Management, 12*(5), 687-704.

Facchetti, A. (2013). Polymer donor–polymer acceptor (all-polymer) solar cells. *Materials Today, 16*(4), 123-132.

Farag, A. A. M., Cavaş, M., Yakuphanoglu, F., & Amanullah, F. M. (2011). Photoluminescence and optical properties of nanostructure Ni doped ZnO thin films prepared by sol–gel spin coating technique. *Journal of Alloys and Compounds, 509*(30), 7900-7908. doi:https://doi.org/10.1016/j.jallcom.2011.05.009

Fell, A., Niewelt, T., Steinhauser, B., Heinz, F. D., Schubert, M. C., & Glunz, S. W. (2021). Radiative recombination in silicon photovoltaics: Modeling the influence of charge carrier densities and photon recycling. *Solar energy materials and solar cells*. doi:10.1016/j.solmat.2021.111198

Frankenstein, H., Leng, C. Z., Losego, M. D., & Frey, G. L. (2019). Atomic layer deposition of ZnO electron transporting layers directly onto the active layer of organic solar cells. *Organic Electronics, 64*, 37-46.

Ghasemi, M., Balar, N., Peng, Z., Hu, H., Qin, Y., Kim, T., . . . McCulloch, I. (2021). A molecular interaction–diffusion framework for predicting organic solar cell stability. *Nature materials, 20*(4), 525-532.

Green, M. A. (2002). Photovoltaic principles. *Physica E: Low-dimensional Systems and Nanostructures, 14*(1-2), 11-17.

Hafdallah, A., Ynineb, F., Aida, M., & Attaf, N. (2011). In doped ZnO thin films. *Journal of Alloys and Compounds, 509*(26), 7267-7270.

Hamed, M. S., Ike, J. N., & Mola, G. T. (2021). Plasmonic nano-particles mediated energy harvesting in thin-film organic solar cells. *Journal of Physics D: Applied Physics, 55*(1), 015102.

Han, B., Gopalan, S.-A., Lee, K.-D., Kang, B.-H., Lee, S.-W., Lee, J.-S., . . . Kang, S.-W. (2014). Preheated solvent exposure on P3HT: PCBM thin film: A facile strategy to enhance performance in bulk heterojunction photovoltaic cells. *Current Applied Physics, 14*(11), 1443-1450.

Han, Y., Dong, H., Pan, W., Liu, B., Chen, X., Huang, R., . . . Zhang, J. (2021). An Efficiency of 16.46% and a T 80 lifetime of over 4000 h for the PM6: Y6 inverted organic solar cells enabled by surface acid treatment of the zinc oxide electron transporting layer. *ACS applied materials & interfaces, 13*(15), 17869-17881.

Hau, S. K., Yip, H.-L., & Jen, A. K.-Y. (2010). A review on the development of the inverted polymer solar cell architecture. *Polymer Reviews, 50*(4), 474-510.

Herzog, A. V., Lipman, T. E., & Kammen, D. M. (2001). Renewable energy sources. *Encyclopedia of life support systems (EOLSS). Forerunner Volume-'Perspectives and overview of life support systems and sustainable development, 76*.

Homnan, S., Malison, P., Amratisha, K., Kanjanaboos, P., Wongratanaphisan, D., Sagawa, T., & Ruankham, P. (2021). Low-temperature processable Sn-doped ZnO films as electron transporting layers for perovskite solar cells. *Journal of Materials Science: Materials in Electronics, 32*, 27279-27289.

Houshyani Hassanzahed, B., van Sark, W., de Keizer, A., Reich, N., Willeke, G., Ossenbrink, H., & Helm, P. (2007). *The Effect of a varying solar spectrum on the energy performance of solar cells.* Paper presented at the 22nd European Photovoltaic Solar Energy Conference.

Hu, T., Chen, L., Yuan, K., & Chen, Y. (2015). Amphiphilic fullerene/ZnO hybrids as cathode buffer layers to improve charge selectivity of inverted polymer solar cells. *Nanoscale, 7*(20), 9194-9203.

Hu, Z., Ying, L., Huang, F., & Cao, Y. (2017). Towards a bright future: polymer solar cells with power conversion efficiencies over 10%. *Science China Chemistry, 60*, 571-582.

Ismail, A. S., Mamat, M. H., Malek, M. F., Saidi, S. A., Yusoff, M. M., Mohamed, R., . . . Rusop, M. (2018). Structural, optical, and electrical properties of Ni-doped ZnO nanorod arrays prepared via sonicated sol-gel immersion method. *AIP Conference Proceedings, 1963*(1). doi:10.1063/1.5036875

Jadhav, J., & Biswas, S. (2016). Shape-controlled magnetic nanoplatelets of Ni-doped ZnO synthesized via a chemical precursor. *Journal of Alloys and Compounds, 664*, 71-82.

Juang, T. Y., Kao, J. C., Wang, J. C., Hsu, S. Y., & Chen, C. P. (2018). Carbonized Bamboo-Derived Carbon Nanodots as Efficient Cathode Interfacial Layers in High-Performance Organic Photovoltaics. *Advanced Materials Interfaces, 5*(10), 1800031.

Jung, S., Lee, J., Kim, U., & Park, H. (2020). Solution-Processed Molybdenum Oxide with Hydroxyl Radical-Induced Oxygen Vacancy as an Efficient and Stable Interfacial Layer for Organic Solar Cells. *Solar RRL, 4*(3), 1900420.

Jung, S., Lee, J., Seo, J., Kim, U., Choi, Y., & Park, H. (2018). Development of annealing-free, solution-processable inverted organic solar cells with n-doped graphene electrodes using zinc oxide nanoparticles. *Nano letters, 18*(2), 1337-1343.

Kamruzzaman, M., Luna, T. R., Podder, J., & Anowar, M. G. M. (2012). Synthesis and characterization of Cd1−xCoxS thin films prepared using the spray pyrolysis technique. *Semiconductor Science and Technology, 27*(3), 035017. doi:10.1088/0268-1242/27/3/035017

Kavitha, M. K., Jinesh, K. B., Philip, R., Gopinath, P., & John, H. (2014). Defect engineering in ZnO nanocones for visible photoconductivity and nonlinear absorption. *Physical Chemistry Chemical Physics, 16*(45), 25093-25100. doi:10.1039/C4CP03847A

Kim, D., Kang, H., Kim, J.-M., & Kim, H. (2011). The properties of plasma-enhanced atomic layer deposition (ALD) ZnO thin films and comparison with thermal ALD. *Applied Surface Science, 257*(8), 3776-3779.

Krebs, F. C. (2009). All solution roll-to-roll processed polymer solar cells free from indium-tin-oxide and vacuum coating steps. *Organic Electronics, 10*(5), 761-768.

Lechêne, B., Leroy, J., Tosoni, O., de Bettignies, R. m., & Perrier, G. r. (2014). Origin of the S-shape upon aging in standard organic solar cells with zinc oxide as transport layer. *The Journal of Physical Chemistry C, 118*(35), 20132-20136.

Lee, T. H., Uddin, M. A., Zhong, C., Ko, S. J., Walker, B., Kim, T., . . . Woo, H. Y. (2016). Investigation of charge carrier behavior in high performance ternary blend polymer solar cells. *Advanced Energy Materials, 6*(19), 1600637.

Lewis, N. S. (2007). Toward cost-effective solar energy use. *Science, 315*(5813), 798-801.

Lewis, N. S., & Nocera, D. G. (2006). Powering the planet: Chemical challenges in solar energy utilization. *Proceedings of the National Academy of Sciences, 103*(43), 15729-15735.

Li, C. Z., Huang, J., Ju, H., Zang, Y., Zhang, J., Zhu, J., . . . Jen, A. K. Y. (2016). Modulate Organic-Metal Oxide Heterojunction via [1, 6] Azafulleroid for Highly Efficient Organic Solar Cells. *Advanced Materials, 28*(33), 7269-7275.

Li, G., Shrotriya, V., Huang, J., Yao, Y., Moriarty, T., Emery, K., & Yang, Y. (2005). High-efficiency solution processable polymer photovoltaic cells by self-organization of polymer blends. *Nature materials, 4*(11), 864-868.

Li, G., Shrotriya, V., Huang, J., Yao, Y., Moriarty, T., Emery, K., & Yang, Y. (2005). Nat. Mater. In.

Li, G., Zhu, R., & Yang, Y. (2012). Polymer solar cells. *Nature photonics, 6*(3), 153-161.

Li, J., Liang, Z., Wang, Y., Li, H., Tong, J., Bao, X., & Xia, Y. (2018). Enhanced efficiency of polymer solar cells through synergistic optimization of mobility and tuning donor alloys by adding high-mobility conjugated polymers. *Journal of Materials Chemistry C, 6*(41), 11015-11022. doi:10.1039/C8TC03612H

Li, J., Ren, M., Qing, J., Wang, Y., Liang, Z., Wang, N., . . . Xia, Y. (2019). Solution-processible Cd-doped ZnO nanoparticles as an electron transport layer to achieve high performance polymer solar cells through improve conductivity and light transmittance. *Molecular Crystals and Liquid Crystals, 692*(1), 74-82.

Li, L., & Schirra, J. S. (2012). H. Cheun, B. Kippelen, OLA Monti, and J.-L. Bredas. *Chemistry of Materials, 24*, 3044.

Liao, S.-H., Jhuo, H.-J., Yeh, P.-N., Cheng, Y.-S., Li, Y.-L., Lee, Y.-H., . . . Chen, S.-A. (2014). Single junction inverted polymer solar cell reaching power conversion efficiency 10.31% by employing dual-doped zinc oxide nano-film as cathode interlayer. *Scientific Reports, 4*(1), 6813.

Liao, S. H., Jhuo, H. J., Cheng, Y. S., & Chen, S. A. (2013). Fullerene derivative-doped zinc oxide nanofilm as the cathode of inverted polymer solar cells with low-bandgap polymer (PTB7-Th) for high performance. *Advanced Materials, 25*(34), 4766-4771.

Liton, M., Khan, K., Rahman, M., & Islam, M. (2015). Effect of N and Cu doping on structure, surface morphology and photoluminescence properties of ZnO thin films. *Journal of scientific research, 7*(1-2), 23-34.

Litzov, I., & Brabec, C. J. (2013). Development of efficient and stable inverted bulk heterojunction (BHJ) solar cells using different metal oxide interfaces. *Materials, 6*(12), 5796-5820.

Lloyd-Jones, L. R., Zeng, J., Sidorenko, J., Yengo, L., Moser, G., Kemper, K. E., . . . Esko, T. (2019). Improved polygenic prediction by Bayesian multiple regression on summary statistics. *Nature communications, 10*(1), 5086.

Luo, Z., Liu, T., Wang, Y., Zhang, G., Sun, R., Chen, Z., . . . Yang, C. (2019). Reduced Energy Loss Enabled by a Chlorinated Thiophene-Fused Ending-Group Small Molecular Acceptor for Efficient Nonfullerene Organic Solar Cells with 13.6% Efficiency. *Advanced Energy Materials, 9*(18), 1900041. doi:https://doi.org/10.1002/aenm.201900041

Mahmood, K., Sarwar, S., & Mehran, M. T. (2017). Current status of electron transport layers in perovskite solar cells: materials and properties. *RSC advances, 7*(28), 17044-17062.

Maldonado, F., & Stashans, A. (2010). Al-doped ZnO: Electronic, electrical and structural properties. *Journal of Physics and Chemistry of Solids, 71*(5), 784-787.

Markham, B., & Barker, J. (1987). Thematic Mapper bandpass solar exoatmospheric irradiances. *International Journal of remote sensing, 8*(3), 517-523.

Martinez-Lozano, J., Tena, F., Onrubia, J., & De La Rubia, J. (1984). The historical evolution of the Ångström formula and its modifications: review and bibliography. *Agricultural and forest meteorology, 33*(2-3), 109-128.

Meng, L., Zhang, Y., Wan, X., Li, C., Zhang, X., Wang, Y., . . . Xia, R. (2018). Organic and solution-processed tandem solar cells with 17.3% efficiency. *Science, 361*(6407), 1094-1098.

Moditswe, C., Muiva, C. M., & Juma, A. (2016). Highly conductive and transparent Ga-doped ZnO thin films deposited by chemical spray pyrolysis. *Optik, 127*(20), 8317-8325.

Moon, B. J., Lee, K. S., Shim, J., Park, S., Kim, S. H., Bae, S., . . . Yi, Y. (2016). Enhanced photovoltaic performance of inverted polymer solar cells utilizing versatile chemically functionalized ZnO@ graphene quantum dot monolayer. *Nano Energy, 20*, 221-232.

Oh, H., Krantz, J., Litzov, I., Stubhan, T., Pinna, L., & Brabec, C. J. (2011). Comparison of various sol–gel derived metal oxide layers for inverted organic solar cells. *Solar energy materials and solar cells, 95*(8), 2194-2199.

Özgür, Ü., Alivov, Y. I., Liu, C., Teke, A., Reshchikov, M., Doğan, S., . . . Morkoç. (2005). A comprehensive review of ZnO materials and devices. *Journal of Applied Physics, 98*(4), 11.

Park, H.-Y., Lim, D., Kim, K.-D., & Jang, S.-Y. (2013). Performance optimization of low-temperature-annealed solution-processable ZnO buffer layers for inverted polymer solar cells. *Journal of Materials Chemistry A, 1*(21), 6327-6334.

Pitchaiya, S., Natarajan, M., Santhanam, A., Asokan, V., Yuvapragasam, A., Ramakrishnan, V. M., . . . Velauthapillai, D. (2020). A review on the classification of organic/inorganic/carbonaceous hole transporting materials for perovskite solar cell application. *Arabian Journal of Chemistry, 13*(1), 2526-2557.

Po, R., Carbonera, C., Bernardi, A., & Camaioni, N. (2011). The role of buffer layers in polymer solar cells. *Energy & Environmental Science, 4*(2), 285-310.

Poduval, G. K., Duan, L., Hossain, M. A., Sang, B., Zhang, Y., Zou, Y., . . . Hoex, B. (2020). High-efficiency nonfullerene organic solar cells enabled by atomic layer deposited zirconium-doped zinc oxide. *Solar RRL, 4*(10), 2000241.

Polydorou, E., Verouti, M., Soultati, A., Armadorou, K.-K., Verykios, A., Filippatos, P.-P., . . . Karatasios, I. (2022). Room-temperature deposited fluorine-doped tantalum pentoxide for stable organic solar cells. *Organic Electronics, 108*, 106607.

Prerna, Arya, S., Sharma, A., Singh, B., Tomar, A., Singh, S., & Sharma, R. (2020). Morphological and optical characterization of sol-gel synthesized Ni-doped ZnO nanoparticles. *Integrated Ferroelectrics, 205*(1), 1-13.

Rafique, S., Abdullah, S. M., Sulaiman, K., & Iwamoto, M. (2018). Fundamentals of bulk heterojunction organic solar cells: An overview of stability/degradation issues and strategies for improvement. *Renewable and Sustainable Energy Reviews, 84*, 43-53.

Rajeh, S., Barhoumi, A., Mhamdi, A., Leroy, G., Duponchel, B., Amlouk, M., & Guermazi, S. (2016). Structural, morphological, optical and opto-thermal properties of Ni-doped ZnO thin films using spray pyrolysis chemical technique. *Bulletin of Materials Science, 39*, 177-186.

Ren, H., Sun, S., Cui, J., & Li, X. (2018). Synthesis, functional modifications, and diversified applications of molybdenum oxides micro-/nanocrystals: A review. *Crystal Growth & Design, 18*(10), 6326-6369.

Rouchdi, M., Salmani, E., el Hat, A., Mzerd, A., & Hassanain, N. (2016). Synthesis and Magnetic Properties of Ni doped ZnO thin films: Experimental and Ab-initio Study. *Surface Review and Letters, 24*. doi:10.1142/S0218625X17500858

Sasajima, I., Uesaka, S., Kuwabara, T., Yamaguchi, T., & Takahashi, K. (2011). Flexible inverted polymer solar cells containing an amorphous titanium oxide electron collection electrode. *Organic Electronics, 12*(1), 113-118.

Schlamadinger, B., Apps, M., Bohlin, F., Gustavsson, L., Jungmeier, G., Marland, G., . . . Savolainen, I. (1997). Towards a standard methodology for greenhouse gas balances of bioenergy systems in comparison with fossil energy systems. *Biomass and bioenergy, 13*(6), 359-375.

Schumann, S., Da Campo, R., Illy, B., Cruickshank, A., McLachlan, M., Ryan, M., . . . Jones, T. (2011). Inverted organic photovoltaic devices with high efficiency and stability based on metal oxide charge extraction layers. *Journal of Materials Chemistry, 21*(7), 2381-2386.

Shafiee, S., & Topal, E. (2009). When will fossil fuel reserves be diminished? *Energy policy, 37*(1), 181-189.

Shin, K.-S., Lee, K.-H., Lee, H. H., Choi, D., & Kim, S.-W. (2010). Enhanced power conversion efficiency of inverted organic solar cells with a Ga-doped ZnO nanostructured thin film prepared using aqueous solution. *The Journal of Physical Chemistry C, 114*(37), 15782-15785.

Song, W., Yu, K., Zhou, E., Xie, L., Hong, L., Ge, J., . . . Ge, Z. (2021). Crumple durable ultraflexible organic solar cells with an excellent power-per-weight performance. *Advanced Functional Materials, 31*(30), 2102694.

Song, X., Liu, G., Gao, W., Di, Y., Yang, Y., Li, F., . . . Zhang, J. (2021). Manipulation of zinc oxide with zirconium doping for efficient inverted organic solar cells. *Small, 17*(7), 2006387.

Stakhira, P., Pakhomov, G., Cherpak, V., Volynyuk, D., Luka, G., Godlewski, M., . . . Hotra, Z. (2010). Photovoltaic cells based on nickel phthalocyanine and zinc oxide formed by atomic layer deposition. *Open Physics, 8*(5), 798-803.

Stubhan, T., Oh, H., Pinna, L., Krantz, J., Litzov, I., & Brabec, C. J. (2011). Inverted organic solar cells using a solution processed aluminum-doped zinc oxide buffer layer. *Organic Electronics, 12*(9), 1539-1543.

Stubhan, T., Salinas, M., Ebel, A., Krebs, F. C., Hirsch, A., Halik, M., & Brabec, C. J. (2012). Increasing the Fill Factor of Inverted P3HT: PCBM Solar Cells Through Surface Modification of Al-Doped ZnO via Phosphonic Acid-Anchored C60 SAMs. *Advanced Energy Materials, 2*(5), 532-535.

Sun, J., Zhu, Y., Xu, X., Lan, L., Zhang, L., Cai, P., . . . Cao, Y. (2012). High efficiency and high V oc inverted polymer solar cells based on a low-lying HOMO polycarbazole donor and a hydrophilic polycarbazole interlayer on ITO cathode. *The Journal of Physical Chemistry C, 116*(27), 14188-14198.

Sutton, R. J. (2018). *Towards stable perovskite materials for photovoltaics.* University of Oxford,

Suwanboon, S., Amornpitoksuk, P., & Sukolrat, A. (2011). Dependence of optical properties on doping metal, crystallite size and defect concentration of M-doped ZnO nanopowders (M= Al, Mg, Ti). *Ceramics International, 37*(4), 1359-1365.

Tao, C., Ruan, S., Zhang, X., Xie, G., Shen, L., Kong, X., . . . Chen, W. (2008). Performance improvement of inverted polymer solar cells with different top electrodes by introducing a MoO 3 buffer layer. *Applied physics letters, 93*(19), 411.

Tegegne, N. (2018). *Photophysics and photovoltaic application of direct heteroarylation derived isoindigo based copolymers.* Stellenbosch: Stellenbosch University,

Tsai, J.-H., Lai, Y.-C., Higashihara, T., Lin, C.-J., Ueda, M., & Chen, W.-C. (2010). Enhancement of P3HT/PCBM photovoltaic efficiency using the surfactant of triblock copolymer containing poly (3-hexylthiophene) and poly (4-vinyltriphenylamine) segments. *Macromolecules, 43*(14), 6085-6091.

Tsai, S., Ho, S., Jhuo, H., Ho, C., Chen, S., & He, J.-H. (2013). Toward high efficiency of inverted organic solar cells: Concurrent improvement in optical and electrical properties of electron transport layers. *Applied physics letters, 102*(25), 253111.

Tu, Q., Cai, D., Wang, L., Wei, J., Shang, Q., Chen, S.-C., . . . Zheng, Q. (2016). Side-chain engineering of diindenocarbazole-based large bandgap copolymers toward high performance polymer solar cells. *Journal of Materials Chemistry C, 4*(25), 6160-6168.

Van Le, Q., Choi, J.-Y., & Kim, S. Y. (2017). Recent advances in the application of two-dimensional materials as charge transport layers in organic and perovskite solar cells. *FlatChem, 2*, 54-66.

Wang, G., Melkonyan, F. S., Facchetti, A., & Marks, T. J. (2019). All-Polymer Solar Cells: Recent Progress, Challenges, and Prospects. *Angewandte Chemie International Edition, 58*(13), 4129-4142. doi:https://doi.org/10.1002/anie.201808976

Wang, J.-C., Weng, W.-T., Tsai, M.-Y., Lee, M.-K., Horng, S.-F., Perng, T.-P., . . . Meng, H.-F. (2010). Highly efficient flexible inverted organic solar cells using atomic layer deposited ZnO as electron selective layer. *Journal of Materials Chemistry, 20*(5), 862-866.

Wang, Y., Lan, W., Li, N., Lan, Z., Li, Z., Jia, J., & Zhu, F. (2019). Stability of nonfullerene organic solar cells: from built-in potential and interfacial passivation perspectives. *Advanced Energy Materials, 9*(19), 1900157.

Wang, Y., Yan, L., Ji, G., Wang, C., Gu, H., Luo, Q., . . . Ma, C.-Q. (2018). Synthesis of N, S-doped carbon quantum dots for use in organic solar cells as the ZnO modifier to eliminate the light-soaking effect. *ACS applied materials & interfaces, 11*(2), 2243-2253.

Wang, Z. L. (2009). Ten years' venturing in ZnO nanostructures: from discovery to scientific understanding and to technology applications. *Chinese Science Bulletin, 54*, 4021-4034.

Wei, J., Ji, G., Zhang, C., Yan, L., Luo, Q., Wang, C., . . . Ma, C.-Q. (2018). Silane-capped ZnO nanoparticles for use as the electron transport layer in inverted organic solar cells. *ACS nano, 12*(6), 5518-5529.

Wei, J., Yin, Z., Chen, S.-C., & Zheng, Q. (2017). Low-temperature solution-processed zinc tin oxide film as a cathode interlayer for organic solar cells. *ACS applied materials & interfaces, 9*(7), 6186-6193.

Wu, Z., Yu, H., Shi, S., & Li, Y. (2019). Bismuth oxysulfide modified ZnO nanorod arrays as an efficient electron transport layer for inverted polymer solar cells. *Journal of Materials Chemistry A, 7*(24), 14776-14789.

Würfel, U., Wagner, J., & Hinsch, A. (2005). Spatial electron distribution and its origin in the nanoporous TiO2 network of a dye solar cell. *The Journal of Physical Chemistry B, 109*(43), 20444-20448.

Xu, H., Yuan, F., Zhou, D., Liao, X., Chen, L., & Chen, Y. (2020). Hole transport layers for organic solar cells: Recent progress and prospects. *Journal of Materials Chemistry A, 8*(23), 11478-11492.

Xu, X., & Peng, Q. (2022). Hole/electron transporting materials for nonfullerene organic solar cells. *Chemistry–A European Journal, 28*(25), e202104453.

Yang, Z., Zhang, T., Li, J., Xue, W., Han, C., Cheng, Y., . . . Chen, S. (2017). Multiple electron transporting layers and their excellent properties based on organic solar cell. *Scientific Reports, 7*(1), 9571.

Ye, J., Gu, S., Qin, F., Zhu, S., Liu, S., Zhou, X., . . . Shi, Y. (2005). Correlation between green luminescence and morphology evolution of ZnO films. *Applied Physics A, 81*, 759-762.

Yildiz, A., Kayhan, B., Yurduguzel, B., Rambu, A., Iacomi, F., & Simon, S. (2011). Ni doping effect on electrical conductivity of ZnO nanocrystalline thin films. *Journal of Materials Science: Materials in Electronics, 22*, 1473-1478.

Yilmaz, M. (2014). Characteristic properties of spin coated ZnO thin films: the effect of Ni doping. *Physica Scripta, 89*(9), 095802.

Yin, Z., Zheng, Q., Chen, S.-C., & Cai, D. (2013). Interface control of semiconducting metal oxide layers for efficient and stable inverted polymer solar cells with open-circuit voltages over 1.0 volt. *ACS applied materials & interfaces, 5*(18), 9015-9025.

Yin, Z., Zheng, Q., Chen, S. C., Cai, D., Zhou, L., & Zhang, J. (2014). Bandgap Tunable Zn1-xMgxO Thin Films as Highly Transparent Cathode Buffer Layers for High-Performance Inverted Polymer Solar Cells. *Advanced Energy Materials, 4*(7), 1301404.

Yu, G. (1995). J., Gao, JC Hummelen, F. Wudi, and A. J Heeger. *Science, 270*, 1789.

Yu, X., Yu, X., Hu, Z., Zhang, J., Zhao, G., & Zhao, Y. (2013). Effect of sol–gel derived ZnO annealing rate on light-trapping in inverted polymer solar cells. *Materials letters, 108*, 50-53.

Yu, X., Yu, X., Zhang, J., Zhao, G., Ni, J., Cai, H., & Zhao, Y. (2014). Efficiency boosting of inverted polymer solar cells with a polyvinylpyrrolidone-modified Al-doped ZnO electron transport layer. *Solar energy materials and solar cells, 128*, 307-312.

Zhang, R., Zhao, M., Wang, Z., Wang, Z., Zhao, B., Miao, Y., . . . Chen, G. (2018). Solution-processable ZnO/carbon quantum dots electron extraction layer for highly efficient polymer solar cells. *ACS applied materials & interfaces, 10*(5), 4895-4903.

Zhao, J., Li, Y., Yang, G., Jiang, K., Lin, H., Ade, H., . . . Yan, H. (2015). Nature Energy 1, 15027 (2016). In.

Zheng, Z., Zhang, S., Wang, J., Zhang, J., Zhang, D., Zhang, Y., . . . Zhou, H. (2019). Exquisite modulation of ZnO nanoparticle electron transporting layer for high-performance fullerene-free organic solar cell with inverted structure. *Journal of Materials Chemistry A, 7*(8), 3570-3576.

Zhu, C., Yuan, J., Cai, F., Meng, L., Zhang, H., Chen, H., . . . Chen, S. (2020). Tuning the electron-deficient core of a non-fullerene acceptor to achieve over 17% efficiency in a single-junction organic solar cell. *Energy & Environmental Science, 13*(8), 2459-2466.

Zhu, X., Hu, L., Wang, W., Jiang, X., Hu, L., & Zhou, Y. (2019). Reversible chemical reactivity of non-fullerene acceptors for organic solar cells under acidic and basic environment. *ACS Applied Energy Materials, 2*(10), 7602-7608.

Zou, Y., Chen, H., Bi, X., Xu, X., Wang, H., Lin, M., . . . Wan, X. (2022). Peripheral halogenation engineering controls molecular stacking to enable highly efficient organic solar cells. *Energy & Environmental Science, 15*(8), 3519-3533.

Research Fund Acknowledgement

This research thesis was funded by Adama Science and Technology University under the grant number of ASTU/SM-R/844/23, Adama, Ethiopia.